CONFIDENTIAL

Copy
RM E52K07



NACA RM E52K07

# RESEARCH MEMORANDUM

## COMPARISON OF PRESSURE-LOSS CHARACTERISTICS OF SEVERAL TAIL-CONE AIR-INDUCTION SYSTEMS FOR AIR-COOLED GAS-TURBINE ROTORS

By Gordon T. Smith and Arthur N. Curren

Lewis Flight Propulsion Laboratory
Cleveland, Ohio



NATIONAL ADVISORY COMMITTEE
FOR AERONAUTICS

WASHINGTON
January 12, 1953

CONFIDENTIAL

NATIONAL ADVISORY COMMITTEE FOR AERONAUTICS

RESEARCH MEMORANDUM

# COMPARISON OF PRESSURE-LOSS CHARACTERISTICS OF SEVERAL TAIL-CONE AIR-INDUCTION SYSTEMS FOR AIR-COOLED GAS-TURBINE ROTORS

By Gordon T. Smith and Arthur N. Curren

## SUMMARY

Three scale models and a full-scale configuration of systems for ducting cooling air through a turbojet engine tail cone to a cooled turbine rotor were investigated in order to determine the pressure-loss characteristics of such systems and to evaluate the effects of these pressure losses on the performance of an air-cooled turbojet engine. The full-scale system and one similar model system were designed primarily on the basis of mechanical simplicity with no regard for the total-pressure losses; the second model was designed to reduce the extreme turbulence of the flow in the discharge duct, which should reduce the pressure losses and improve the reliability of pressure measurements at the entrance to the cooled turbine rotor; and the third made a substantial sacrifice of mechanical simplicity in order to reduce the over-all total-pressure losses.

The total-pressure losses through the configurations were evaluated experimentally in the form of a pressure-loss ratio and were compared over a range of discharge-duct Mach numbers. The results were also compared with calculated total-pressure losses through the model configurations. These measurements indicated that the third configuration was the most effective with respect to pressure loss, the ratios for the first and second being about 300 and 400 percent higher, respectively, than that for the third configuration. The calculated pressure losses through the model configurations were consistently lower than the experimental values, which indicates that the design of the cooling-air bleed system based on calculated pressure losses should be conservative in order to ensure an adequate supply of cooling air to the cooled turbine rotor.

The calculated thrust and specific fuel consumption are presented for an uncooled engine and for two air-cooled engines with different pressure-loss levels in the cooling-air bleed system. The calculated effect of the cooling-air pressure losses on engine thrust and specific fuel consumption was in agreement with the results of previous calculations, in that in engines using coolant-flow ratios of about 2 to 4 percent these values were substantially unaffected by the pressure losses

in the cooling-air bleed system. For this type engine, therefore, it is not necessary to sacrifice mechanical simplicity in order to gain good pressure-loss characteristics of the cooling-air system, except where these refinements are necessary in order that the pressure available from the engine compressor can satisfy the cooling requirements of the cooled turbine rotor.



## INTRODUCTION

In a turbojet engine having an air-cooled turbine it is necessary to duct the cooling air from some high-pressure source to the cooling-air inlet of the turbine. One of the many methods for ducting this air (a few of which are discussed in reference 1) that has been employed by the NACA in its turbine-cooling research is the introduction of the air through a system built into the tail cone of the engine (reference 2). The cooling-air ducting system of reference 2 was designed primarily on the basis of mechanical simplicity; and, because good pressure-loss characteristics are generally not compatible with mechanical simplicity, the pressure losses in this system were large. For applications where the pressure requirements at the hub of the cooled turbine rotor are near the maximum pressures available by bleeding the engine compressor, or where large cooling-air flows are required, it will be necessary to minimize and predict accurately the cooling-air pressure losses in the bleed system which supplies the cooling air to the turbine rotor. For this reason, research on tail-cone air-induction systems other than the system of reference 2 is desirable.

The results of reference 3 indicate that, for the range of coolant-flow ratios that will probably be tolerated for turbine cooling with air, the required cooling-air pressure at the entrance to the rotor is less than compressor-discharge pressure. For flight application, therefore, it appears that the most likely source of cooling air for turbine cooling will be the main engine compressor, provided pressure losses in the ducting between the compressor and the turbine rotor are not excessive. Reduction of these losses in the ducting may be important, particularly for multistage compressors, because it permits bleeding the cooling air from the earlier stages, which will reduce both the cooling-air temperature and the compressor work. Reduction of cooling-air temperature reduces the quantity of cooling air required for adequate turbine cooling, and smaller amounts of cooling air result in minimum losses in engine performance due to cooling.

The calculations of reference 4, which represent the two limiting levels of pressure loss in the engine bleed system, were made for both cooling air bled from the engine compressor at the pressure required at the entrance to the cooled turbine rotor and for cooling air bled at the discharge of the engine compressor. The first case represents the

condition of negligible pressure losses in the cooling-air bleed system, and the second condition represents the maximum pressure loss in the cooling-air bleed system which will still permit adequate cooling of the turbine rotor. These results indicate that for engines using coolant-flow ratios up to 3 percent, the losses in engine thrust and specific fuel consumption that can be attributed to pressure losses in the bleed system are about 1 percent. For applications where more severe cooling requirements demand significantly higher cooling-air flows than were considered in reference 4, the engine-performance penalties associated with the pressure losses in the cooling-air supply system would be more significant.

In order to obtain a better understanding of the pressure-loss characteristics in tail-cone cooling-air ducting systems, three different scale-model ducting configurations and one full-scale tail-cone ducting system similar to one of the models were experimentally investigated at the NACA Lewis laboratory in order to measure and compare the pressure losses for each configuration. These losses were also calculated for each tail-cone system by conventional pressure-loss formulas.

The present report provides information which will be helpful in the design of an air-cooled engine coolant system. The following four factors are discussed: (1) the magnitude of the cooling-air pressure losses in three different model tail-cone ducting systems and a comparison of the losses in one scale model with the losses in a full-scale tail-cone system, (2) the comparison of the experimentally determined losses with the losses calculated from conventional pressure-loss formulas, (3) the effects of these pressure losses on the performance of an air-cooled turbojet engine, and (4) the extent to which mechanical simplicity should be compromised in favor of aerodynamic refinement of a cooling-air ducting system. Experimental and calculated pressure losses were determined for cooling-air Mach numbers at the inlet of the turbine rotor from 0 to about 0.6.

## APPARATUS AND INSTRUMENTATION

The three model ducting systems were fabricated to approximately one-third scale, the full-scale size being based upon conventional tail-cone size and expected coolant-flow needs. The model tail-cone cooling-air systems were operated at subatmospheric pressure and inducted air directly from the test cell; the full-scale configuration, at a pressure level higher than atmospheric, the cooling air being supplied by the laboratory pressure-air system.

Tail-Cone Air-Induction-System Configurations

Full-scale configuration. - The full-scale air-induction system investigated is shown in figure 1. Four primary-cooling-air supply tubes passed through the tail-cone struts and discharged abruptly and perpendicularly into a circular-section central delivery tube which supplied cooling air to the turbine rotor. The cross-sectional area of this central delivery tube equalled the combined cross-sectional area of the primary inlet tubes, which were located in diametrically opposite pairs, one pair 1.5 diameters downstream on the central delivery tube from the other and all on the same axial plane through the central delivery tube. This configuration had been utilized previously in full-scale turbojet-engine air-cooled turbine-rotor investigations (reference 2) and had been fabricated by the alteration of a standard engine tail cone. The engine for which this configuration was designed utilized a high-pressure source of cooling air external to the engine and was not concerned with the pressure losses of the cooling-air system. For this reason, the full-scale system was designed primarily from considerations of mechanical simplicity, and no effort was made to minimize the cooling-air pressure losses.

Model A. - The first model system investigated was model A (fig. 2(a)), a one-third-scale reproduction of the full-scale configuration described previously, chosen because of the previous use of the prototype and because the existence of the prototype made possible comparison tests between it and the model. The model was fabricated of common plaster of Paris cast in a wooden form, with cores of easily removable material. Plaster of Paris was chosen for the casting medium because of its availability, the comparative ease with which it may be controlled, and because it casts to a smooth, hard surface. Since model A was composed of elementary geometrical shapes, simple cores of greased balsa wood dowels, which were easily withdrawn after the plaster had become hard, were used. A short pipe coupling was cast into the model, at the outlet station, in order to facilitate easy attachment to an extension of the central delivery tube. The air passage past the coupling was smooth, so that the air flow was unaffected by its presence.

Model B. - Model B (fig. 2(b)) was proposed as an improvement over model A, which exhibited considerable flow instability in full-scale investigations and caused pressure measurements taken in the central delivery tube to fluctuate. Model B featured a relatively large calming chamber, which was supplied by two diametrically opposed primary supply tubes of elliptical cross section, which supplied the central coolant delivery tube leading to the turbine rotor. The calming chamber had the shape of a frustum of a right cone, and the two primary supply tubes intersected the sides of the chamber at right angles to, and at one-half the length of the axis of the frustum. The major axes of the elliptical primary supply tubes were parallel to the axis of the chamber, and the

[redacted]

central delivery tube joined the base, the largest-diameter section, of the chamber on the axis of the chamber and perpendicularly to the primary-air supply tubes. The base of the chamber was generously faired to the entrance of the central delivery tube in order to minimize entrance losses. The calming chamber was expected to reduce the large amount of turbulence giving rise to the flow instabilities of the design of model A. The primary-air supply tubes were elliptical in cross section in order that the tail-cone strut through which these tubes must enter the inner cone could be sufficiently narrow to prevent excessive reduction in the combustion-gas-flow area (fig. 1). The calming chamber was designed to conform to the interior shape of this inner cone so that the chamber could be of maximum volume. A set of removable straightening vanes, 1.5 diameters long, was located at the exit to the calming chamber to reduce further the flow instabilities at the downstream instrumentation station. Model B was investigated both with and without these straightening vanes in the discharge tube. The method of fabricating model B was similar to that of model A, except that a different coring material was used. Because it involved more complex interior shapes than model A, model B utilized a molded paraffin core which was melted out of the plaster block after the plaster had solidified.

Model C. - The model C configuration (fig. 2(c)) utilized two primary supply tubes of elliptical cross section which brought the cooling air from opposite sides of the model. These tubes were curved 90° about their minor cross-sectional axis, so that the air was discharged axially into the circular cross-sectional delivery tube leading to the turbine rotor. This model was fabricated in a manner similar to that previously described, and again a core of molded paraffin was used.

## Air Supply Systems

Full-scale configuration. - High-pressure air, supplied by the laboratory high-pressure-air supply system, was passed through the full-scale air-induction system and discharged at atmospheric pressure. A throttle valve which regulated the air flow was located upstream of the air-induction system.

Model configurations. - In the model investigations, the laboratory altitude exhaust system was utilized as a test facility. Air was drawn from the test cell, at room conditions, into the model air-induction systems, and then into the vacuum exhaust system. The flow rate through the entire system was regulated by means of a throttle valve located downstream of the model position (fig. 3).



[redacted]

## Instrumentation

Full-scale configuration. - Locations of instrumentation used to determine the pressure-loss characteristics of the full-scale system are shown in figure 4. The inlet static pressures were measured by wall taps located in the primary-air inlet tubes at a point 9.3 diameters upstream of the point where the inlet-air tubes discharged into the discharge duct. The cooling-air inlet temperature was measured by thermocouples installed in the inlet-air tubes. The discharge conditions were measured in the central discharge tube at a point 1.8 diameters axially downstream of the center line of the first pair of primary-air inlet supply tubes. The distribution of the total pressure was determined by three total-pressure tubes and two static wall taps. The temperature in the discharge tube was measured by two thermocouples located on the same rake with the total-pressure probes, and the weight flow was measured by a standard A.S.M.E. orifice located in the air supply line upstream of the tail-cone configuration. These temperature and weight-flow measurements in connection with the static wall pressures permitted an additional determination of the average total pressure in the discharge duct.

Model configurations. - Locations of instrumentation used to determine the pressure-loss characteristics of the model configurations are shown in figure 3. The temperature and pressure of the air entering the primary-air inlet tubes was measured with a mercury thermometer and a standard barometer. In model A the total-pressure probe on the center line of the discharge tube and the pair of wall static-pressure taps were located 10 tube diameters downstream of the center line of the first pair of primary-air inlet tubes as shown in figure 3. In models B and C, these measurements were made 11 diameters downstream of the center line of the primary-air inlet tubes. In all model configurations a total-pressure survey probe was located 1.25 diameters upstream of the station where the center-line total pressure and static wall pressures were measured.

The locations of the pressure-measuring instrumentation were necessarily different between model A and the full-scale configuration. The short discharge-tube length of the full-scale configuration required that the measurements of discharge total and static pressures be made quite close to the transition section. These measurements were made farther downstream in the discharge tube of the models in order to permit a more reliable measurement of the discharge pressures in the more stable downstream region. The measured inlet pressures for model A were the ambient pressure conditions of the test cell, and the inlet conditions of the full-scale configuration were the measured temperatures and static pressures in the primary-air inlet tubes. These differences in locations of the instrumentation were not expected to influence materially the overall comparisons between model A and the full-scale tail-cone configuration,

because the differences in the friction and mixing losses between the measuring stations of the two configurations were expected to be very small in comparison with the over-all total-pressure loss through each configuration.



## EMPIRICAL FORMULAS FOR DUCT PRESSURE LOSSES

### Individual Losses

The total-pressure losses in most duct systems can be approximated from established empirical formulas and data that are readily available in the literature. For the various tail-cone cooling-air ducting systems considered herein, the over-all total-pressure losses throughout the systems can be considered to be made up of a number of individual total-pressure losses, such as entrance, friction, expansion, contraction, and bend losses. In the following discussion, all of the equations were obtained from reference 5, except those pertaining to entrance and bend losses, which were obtained from references 6 and 7, respectively. The equations of these references have been converted to the notation of this report, and in all cases they are for turbulent flow unless otherwise indicated. The equations also consider that the fluid is incompressible.

Entrance loss. - The expression for the total-pressure loss due to entrance effects, when the flow area before the entrance is very much larger than the duct immediately downstream of the entrance, is

$$\Delta p'_{en} = K_{en} \frac{\rho_d V_d^2}{2g} \tag{1}$$

(All symbols are defined in the appendix.) The value of the entrance loss coefficient $K_{en}$ depends upon the type of entrance (sharp edge, slightly rounded, well rounded, etc.) and can be obtained from reference 6. The values of specific weight $\rho_d$ and velocity $V_d$ of equation (1) are evaluated for conditions downstream of the entrance.

Friction loss. - The total-pressure loss in a straight length of constant-diameter ducting can be expressed as

$$\Delta p'_f = f_{av} \frac{l}{d} \left( \frac{\rho V^2}{2g} \right)_{av} \tag{2}$$

where $\left( \frac{\rho V^2}{2g} \right)_{av}$ is the average value of the velocity head for the length $l$ of the duct being considered, and $d$ is the hydraulic diameter of the

[redacted]

duct. The local value of the friction factor $f$ can be calculated for Reynolds numbers up to 150,000 by the Blasius formula

$$f = \frac{0.316}{Re^{0.25}} \tag{3a}$$

and for Reynolds numbers above this value by the following equation from reference 5:

$$f = 0.0056 + 0.500\ Re^{-0.32} \tag{3b}$$

The value of Reynolds number is obtained from the expression

$$Re = \frac{W_a}{A}\frac{d}{\mu g} \tag{4}$$

Expansion losses. - In duct systems where there is a sudden enlargement in the cross-sectional area of the duct, the total-pressure loss can be expressed as

$$\Delta p'_{ex} = K_{ex}\frac{\rho_u V_u^2}{2g} \tag{5}$$

The density and the velocity are evaluated upstream of the expansion. The value of the expansion coefficient $K_{ex}$ may be expressed as

$$K_{ex} = \left(1 - \frac{A_u}{A_d}\right)^2 \tag{6}$$

where $A_u$ is the area of the duct upstream of the point of expansion and $A_d$ is the area of the duct downstream of this point.

Contraction losses. - For a sudden contraction in a duct system the total-pressure loss can be expressed as

$$\Delta p'_c = K_c\frac{\rho_d V_d^2}{2g} \tag{7}$$

The value of the contraction coefficient $K_c$ may be expressed as

$$K_c = \left(\frac{1}{C_c} - 1\right)^2 \tag{8}$$

The value of $C_c$ is an experimentally determined value of the ratio of the area of the vena contracta to the area of the smaller duct. The value of $C_c$ is a function of $A_d/A_u$, where $A_d$ and $A_u$ are the cross-sectional areas downstream and upstream of the contraction, respectively. Values of $C_c$ can be obtained from reference 5.

Bend losses. - The total-pressure losses associated with a change in flow direction of the fluid in a duct system can be represented by

$$\Delta p_b' = f \frac{l_{eq}}{d} \frac{\rho_d V_d^2}{2g} \tag{9}$$

The value of the friction factor f in equation (9) is obtained in the same manner as previously indicated by equation (3a), and $l_{eq}$ is the equivalent length of straight duct required to produce the same pressure loss as the bend. The value of $l_{eq}$ is obtained experimentally, and values of $l_{eq}$ for various types of bend can be obtained from reference 6. Equation (9) is usually written in the form

$$\Delta p_b' = K_b \frac{\rho_d V_d^2}{2g} \tag{9a}$$

where $K_b$ replaces $f \frac{l_{eq}}{d}$ of equation (9).

Compressibility and Reynolds number effects. - Equation (3a), which is used to determine the value of the friction factor f in equations (2) and (9), assumes that the friction factor is only a function of Reynolds number. The effect of compressibility, or Mach number, is not considered. It is known that friction factors for supersonic flow are different from those for subsonic flow and that there is some variation with Mach number even in the subsonic region at high Mach numbers. For the range of Mach numbers encountered in the present investigation, however, the change in friction factor would be so small as to be negligible; and, consequently, compressibility effects were neglected.

The effect of the internal heating caused by the viscous dissipation of total-pressure energy on the pressure losses in the system is generally sufficiently small that it can be properly neglected. If the equivalent length over diameter of the system multiplied by the average friction factor $f_{av} \frac{l_{eq}}{d}$ is below 5 and the inlet Mach number is below 0.2, these effects will be insignificant. Otherwise, compressible-flow methods such as those of reference 5 should be used, if an accurate determination of the pressure loss is desired. These compressibility effects are neglected in this report.

The values of the loss coefficient K in equations (1), (5), and (7) are determined primarily by the geometry of the ducting system. Frequently the loss coefficients are relatively constant over a wide range of Reynolds numbers. Reference 7 indicates that for some duct configurations there is a variation in the value of K with Reynolds number, particularly in the range of Reynolds numbers below $2 \times 10^5$. The

Reynolds numbers for most of the flows in the model systems of this report are below this value; however, there is little information available in the literature regarding the variation of the loss-coefficient Reynolds number below $2\times10^5$. Because the Reynolds number effect is of secondary importance in determining the value of the loss coefficient and because data for determining the variation of the loss coefficient with Reynolds number were not readily available, Reynolds number effects on the value of K have been disregarded in this report.



## Correlation of Total-Pressure Losses for Duct System

In the previous section, standard equations were presented that permit the evaluation of duct pressure losses caused by friction, and pressure losses caused by entrance effects, expansions, contractions, and bends. The latter group of losses are generally called mixing losses.

For a section of a duct system, the pressure loss caused by friction can be written from equation (2) as

$$\Delta p'_{x,f} = f_x \frac{l_x}{d_x} \frac{\rho_x V_x^2}{2g} \tag{10}$$

and the pressure loss caused by mixing effects for any section x can be written from equations (1), (5), (7), and (9a) as

$$\Delta p'_{x,s} = K_x \frac{\rho_x V_x^2}{2g} \tag{11}$$

If the system under consideration is composed of a number of different component sections x having different flow areas, equations (10) and (11) can be rewritten from continuity considerations for any of the sections as

$$\Delta p'_{x,f} = f_x \frac{l_x}{d_x} \frac{A_r^2}{A_x^2} \frac{w^2}{2g\rho_x A_r^2} \tag{10a}$$

and

$$\Delta p'_{x,s} = K_x \frac{A_r^2}{A_x^2} \frac{w^2}{2g\rho_x A_r^2} \tag{11a}$$

The subscript r denotes an arbitrary reference station in one of the duct-system components.

[redacted]

If the density in the duct system does not change appreciably and it can be considered a constant, equations (10a) and (11a) can be rewritten

$$\Delta p'_{x,f} = \left( f_x \frac{l_x}{d_x} \frac{A_r^2}{A_x^2} \right) \frac{\rho_r V_r^2}{2g} \tag{10b}$$

and

$$\Delta p'_{x,s} = \left( K_x \frac{A_r^2}{A_x^2} \right) \frac{\rho_r V_r^2}{2g} \tag{11b}$$

The over-all total-pressure loss in the duct system can then be indicated by

$$\Delta p'_o = \left( \sum f_x \frac{l_x}{d_x} \frac{A_r^2}{A_x^2} + \sum K_x \frac{A_r^2}{A_x^2} \right) \frac{\rho_r V_r^2}{2g} \tag{12}$$

where the first term in the parentheses is a summation of the friction losses in the system, and the second term is a summation of the losses caused by secondary flows.

If, for purposes of obtaining a method of correlating pressure-drop data in a tail-cone ducting system, the pressure drop is evaluated from the inlet of the tail cone (station 8 in fig. 5 for the full-scale tail cone or ambient test-cell conditions for the scale models) to the cooling-air inlet of the turbine rotor (station 9 for both full-scale and model tail cones) equation (12) can be rewritten in terms of Mach number as follows:

$$\rho_r = \frac{p_r}{RT_r} \tag{13}$$

and

$$M_r^2 = \frac{V_r^2}{\gamma_r g R T_r} \tag{14}$$

or

$$V_r^2 = \gamma_r g R T_r M_r^2 \tag{14a}$$

By substituting equations (13) and (14a) in equation (12), the value of $\rho_r V_r^2/2g$ becomes $p_r \gamma_r M_r^2/2$ and equation (12) can be expressed for the full-scale tail cone as

[redacted]

$$\frac{\Delta p'_{8,9}}{p_9} = \left( \sum_{8-9} f_x \frac{l_x}{d_x} \frac{A_9^2}{A_x^2} + \sum_{8-9} K_x \frac{A_9^2}{A_x^2} \right) \frac{\gamma_9}{2} M_9^2 \qquad (12a)$$

and for the tail-cone models as

$$\frac{\Delta p'_{am-9}}{p_9} = \left( \sum_{am-9} f_x \frac{l_x}{d_x} \frac{A_9}{A_x^2} + \sum_{am-9} K_x \frac{A_9^2}{A_x^2} \right) \frac{\gamma_9^2}{2} M_9^2 \qquad (12b)$$

In the section on individual pressure losses it was assumed that the values of the friction factors $f$ in equations (2) and (9) were a function of Reynolds number only and that the loss coefficients for entrances, expansions, and contractions ($K_{en}$, $K_{ex}$, and $K_c$) that appear in equations (1), (5), and (7) were functions of the duct geometry only. From equation (3a) it can be seen that a relatively large change in Reynolds number will result in a comparatively small change in the value of $f$; therefore, the total-pressure loss as calculated by equations (2) and (9) will not be appreciably in error because of a change in Reynolds number.

Furthermore, the values of $fl/d$ for the duct systems considered herein are very small compared with the values of $K$ that are used. The small change in $fl/d$ that would occur with change of Reynolds number would, consequently, affect the over-all pressure losses very little. The assumption can then be made that $f_x l_x/d_x$ for each section of the tail-cone induction system is constant, and then, from equations (12a) and (12b), the pressure losses are functions only of Mach number at station 9.

Station 9 was selected as the reference station, because in an air-cooled turbine design the designer would probably first determine the pressure changes through the cooled blades and disks from known conditions at the blade tips. In this manner the required pressure level at the cooling-air inlet to the rotor (station 9) would be obtained, and the tail-cone duct system, from pressure-loss considerations, would be designed to meet the pressure requirements at station 9.

## ANALYSIS OF EFFECT OF TAIL-CONE COOLING-AIR-INDUCTION-SYSTEM PRESSURE LOSSES ON ENGINE PERFORMANCE

In the following sections the method of analysis that is used to determine the effects of cooling-air-duct-system pressure losses on engine performance for a turbojet engine incorporating a compressor bleed system is discussed.

## Determination of Cooling-Air-Flow Rate and Compressor Bleed Pressure and Temperature

The coolant flow $w_a$ required to cool a turbine blade to a given temperature $T_B$ depends upon the effective combustion-gas temperature $T_{g,e}$, the effective cooling-air temperature at the blade base $T_{e,10}$, and the cooling effectiveness (heat-transfer characteristics) of the blade. The cooling-air total pressure required at the compressor (station 7, fig. 5) to maintain a given coolant flow depends upon the total-pressure losses in the cooling-air ducting system between the compressor and the tail-cone entrance $(\Delta p'_{7-8})$, the total-pressure losses in the tail-cone duct system $(\Delta p'_{8-9})$, the total-pressure changes in the turbine disk and blades $(\Delta p'_{9-4})$, and upon the combustion-gas pressure that exists at the blade tips $(p'_4)$.

The cooling effectiveness of an air-cooled turbine blade provides a relation between the blade temperature, the effective combustion-gas temperature, the effective cooling-air temperature at the blade base, the combustion-gas flow $w_g$ and the cooling-air flow $w_a$, that can be expressed as

$$\frac{T_{g,e} - T_B}{T_{g,e} - T_{e,10}} = \xi^{I}\left(\frac{w_a}{w_g}\right) \tag{15}$$

The variation of the ratio $\frac{T_{g,e} - T_B}{T_{g,e} - T_{e,10}}$, hereinafter defined as $\varphi$, with $w_a/w_g$ for a given cooled turbine-blade configuration can be determined experimentally as discussed in reference 8. In general, the values of $T_B$, $T_{g,e}$, and $w_g$ are fixed by the specific engine design being considered, and as a result equation (15) for a specific blade configuration can be expressed

$$w_a = \xi^{II}(T_{a,10}) \tag{16}$$

The specific engine design being considered will also establish the total temperature and total pressure of the cooling air at the inlet to the rotor hub ($T'_9$ and $p'_9$, respectively) and the cross-sectional area of tail-cone duct system at the rotor hub inlet $A_9$. From the values of $w_a$, $p'_9$, $T'_9$, and $A_9$, the values of the Mach number and static pressure at the rotor hub inlet $M_9$ and $p_9$, respectively, can be found. When the values of Mach number, temperature, and pressure at the rotor hub inlet are established and the total-pressure losses and cooling-air

temperature changes in the cooling-air duct system between the compressor and the rotor hub inlet are known, the required pressure at the compressor $p'_7$ and the associated total temperature $T'_7$ can be determined.

The detailed calculations for determining the various pressures, temperatures, and weight flows discussed in this analysis will be presented in the section CALCULATION PROCEDURE.



Determination of Effect of Pressure Losses on Engine Performance

When the cooling-air flow and the associated required compressor bleed-system pressure are known for a given cooling-air ducting system, the effect of these quantities on engine thrust and specific fuel consumption can be established. Determination of the engine thrust requires knowledge of the temperature and the pressure at the inlet to the tailpipe nozzle, and determination of the specific fuel consumption requires knowledge of the fuel flow.

The total temperature at the compressor outlet $T'_2$, the total temperature at the turbine inlet $T'_3$, and the amount of air leaving the compressor $w_A - w_a$ are established by the engine design, so that the fuel-air ratio $f$ and, consequently, the fuel flow can be determined from the following equation and the charts of reference 9:

$$f = \frac{h'_{0,3} - h'_{0,2}}{\eta_b H - h'_{0,3} - \psi_{h,3} + h_F} \tag{17}$$

In equation (17), $h'_0$ is the enthalpy of dry air for zero fuel-air ratio at the total temperature of the station being considered; $\eta_b$ is the burner efficiency; $H$ is the lower heating value of the fuel; $h_F$ is the enthalpy of the fuel; and $\psi_h$ is defined in reference 9 as $\frac{(h' - h'_0)(1 + f)}{f}$. Values of $h'_0$ and $\psi_h$ for various temperatures and for fuels of various hydrogen-carbon ratios are given in reference 9.

In order to obtain the total pressure and temperature in the tail pipe, it is necessary first to determine the specific turbine work $\Omega$, or the work done by each pound of turbine combustion-gas flow. This value can be obtained by equating the turbine work to the compressor work plus the work done by the turbine rotor on the cooling air in the interior of the turbine rotor. The compressor work consists of two parts, the work done on the cooling air $w_a \frac{c_{p,1} T'_1}{\eta_C} \left[ \left( \frac{p'_7}{p'_1} \right)^{\frac{\gamma - 1}{\gamma}} - 1 \right]$ and the

[redacted]

work done on the combustion air $\frac{(w_A - w_a)c_{p,1}T_1'}{\eta_C}\left[\left(\frac{p_2'}{p_1'}\right)^{\frac{\gamma-1}{\gamma}} - 1\right]$. The work done by the turbine rotor in bringing the cooling air from the rotor hub to the blade tips is $w_a\left(\frac{\omega^2 r^2}{gJ}\right)$. The equation for the specific turbine work can therefore be expressed by

$$\Omega = \frac{\left(\frac{w_a}{w_A - w_a}\right)\frac{c_{p,1}T_1'}{\eta_C}\left[\left(\frac{p_7'}{p_1'}\right)^{\frac{\gamma-1}{\gamma}} - 1\right] + \frac{c_{p,1}T_1'}{\eta_C}\left[\left(\frac{p_2'}{p_1'}\right)^{\frac{\gamma-1}{\gamma}} - 1\right] + \left(\frac{w_a}{w_A - w_a}\right)\left(\frac{\omega^2 r^2}{gJ}\right)}{\frac{w_g}{w_A - w_a}} \tag{18}$$

where $w_g = w_A - w_a + w_F$. For this analysis all the quantities in this expression are known from the engine design or can be determined from methods discussed previously.

The total temperature and the total pressure immediately downstream of the turbine $T_5'$ and $p_5'$, respectively, can now be determined from the expressions

$$\Omega = c_{p,3}\,(T_3' - T_5') \tag{19}$$

and

$$\Omega = c_{p,3}\,T_3'\left[1 - \left(\frac{p_5'}{p_3'}\right)^{\frac{\gamma_3-1}{\gamma_3}}\right]\eta_T \tag{20}$$

The calculations of reference 4 indicate that the change in total temperature and total pressure due to the mixing of the cooling air with the combustion gas between station 5 and the entrance to the tail-pipe nozzle was negligible for coolant-flow ratios below 3 percent. If this assumption is made, $T_5'$ and $p_5'$ can be used to evaluate the jet velocity $V_6$:

$$V_6 = \left\{\left[\left(\frac{p_5'}{p_0}\right)^{\frac{\gamma_5-1}{\gamma_5}} - 1\right](2gc_pJT_5')\right\}^{\frac{1}{2}} \tag{21}$$

[redacted]

The engine thrust F can then be determined from the equation

$$F = \left(\frac{w_g + w_a}{g}\right)(V_6 - V_0) \tag{22}$$

and the engine specific fuel consumption becomes

$$sfc = \frac{3600\ w_F}{F} \tag{23}$$

where $w_F = (f)(w_A - w_a)$, and f is determined by equation (17).



## EXPERIMENTAL PROCEDURE

### Investigation of Full-Scale Tail-Cone Air-Induction System

An investigation of the pressure losses in the full-scale cooling-air-induction system was made in order to obtain a comparison of the full-scale losses with those of a similar scale-model configuration. The losses of the full-scale configuration were obtained for two different levels of pressure in the tail-cone system in order to establish the effect of pressure level on the pressure-loss comparisons.

For the low-pressure-level runs, the cooling air from the full-scale system was discharged directly into the test cell. For the higher pressure runs, the full-scale tail cone was attached to an air-cooled turbojet engine as indicated in figure 1. Cooling air was then passed through the air-induction system and discharged into the static air-cooled turbine rotor. The pressure losses experienced by the cooling air passing through the static turbine-rotor disk and blades were thereby employed to raise the level of the cooling-air pressures in the air-induction system. For both the restricted and unrestricted outlet runs, the cooling-air weight flow was varied from zero to about 4.5 pounds per second in about 20 increments by a remotely controlled throttle valve located upstream of the tail-cone system. The absolute static pressure in the discharge duct of the tail cone varied from 29.12 to 41.77 inches of mercury for the unrestricted outlet runs and from 30.81 to 74.66 inches of mercury for the restricted outlet runs.

For each run, the cooling-air weight-flow rate was determined by a standard A.S.M.E. sharp-edge orifice located in the inlet piping system upstream of the throttle valve and the tail-cone system. The static pressure and the effective temperatures were measured in the inlet tubes immediately upstream of the tail cone by a static wall tap and a thermocouple probe as shown in figure 4. The conditions in the discharge duct were established by measurements of the effective cooling-air temperature, the total pressures, and the wall static pressures, also indicated in figure 4.

### Investigation of Model Air-Induction System

The pressure losses through the three model air-induction systems were determined by inlet and exit pressure measurements. The air was drawn from the test cell in which the models were located and through the model configurations by means of the laboratory altitude exhaust system. The weight-flow rate through the models was controlled by a hand-operated control valve located in the discharge duct of the models (fig. 3). The weight-flow rate was varied from zero flow to the maximum attainable value of about 0.18 pound per second in 10 steps. The static pressure in the discharge duct varied from about 21.5 inches of mercury at the high flow rate to barometric pressure at zero weight flow. On each run the following measurements were taken (see fig. 3):

(1) Total pressure on center line of discharge duct about 10 diameters downstream of center line of primary-air inlet tubes

(2) Static wall pressures at same axial location

(3) Temperature of air in test cell near inlet of model primary-air inlet tubes

(4) Pressure in test cell (which was atmospheric)

On two of the test runs of models A and B and on each run of model C, a survey of the total pressure in the discharge duct was taken about 9 diameters downstream of the center line of the primary-air inlet tubes (see fig. 3). In order to locate the position in the duct at which each total pressure would be measured, the flow area of the discharge duct was divided into five equal-area annuli, and the total pressure was measured at a radius equal to the mean radius of each individual annulus. Thus a total of 10 pressure measurements was obtained across the diameter of the duct.

## CALCULATION PROCEDURE

### Pressure Losses from Experimental Data

The results of the pressure-loss analysis indicated that the pressure losses through a ducting system could be correlated by expressing the pressure-loss ratio as a function of the Mach number in the discharge duct as shown by equations 12(a) and 12(b). In order to evaluate these quantities the following calculations were made.

Full-scale air-induction system. - The evaluation of the pressure-loss ratio $\frac{\Delta p'_{8-9}}{p_9}$ that appears in equation 12(a) for the full-scale

[redacted]

tail cone involved the determination of the pressures in this quantity. The average inlet total pressure $p'_{av,8}$ was determined from the measurements of static pressure and effective cooling-air temperature at the inlet to the tail-cone induction system and from the cooling-air weight flow. From these measurements a static-pressure parameter $\left(\frac{pA}{w_a\sqrt{gRT'}}\right)_8$ was calculated. From this parameter and the compressible-flow charts of reference 10, the total pressure was determined. The cooling-air weight flow, which was measured in a single orifice run upstream of the tail cone, was assumed to divide equally among the four primary-air inlet tubes. The indicated temperature at station 8 was used as the true total temperature in these calculations, because correcting the indicated temperature by means of a recovery factor produced no significant change in the calculated average total pressure.

The average total pressure in the discharge duct $p'_{av,9}$ was determined by a calculation procedure identical to the one used to establish the inlet total pressure. This calculation used the measurements of static pressure, weight flow, and effective temperature at station 9 in the manner previously described. As before, the measured effective temperatures were used as equivalent to the true total temperature in the calculation.

The measurement of three total pressures and two wall static pressures in the discharge duct permitted an independent determination of the average total pressure in the discharge duct which was used as a cross check on the average total pressure computed by the preceding method. Preliminary checks at the start of the investigation indicated that good agreement between the calculated and measured average total pressure in the discharge duct was obtained. Because the average total pressures based on weight-flow measurements were considered more accurate than the fluctuating total-pressure measurements obtained in the discharge duct, the calculated average total pressures were used in this investigation.

In order to make a comparison between the pressure losses in a model air-induction system and the similar full-scale system, it was necessary to add an entrance loss to the total-pressure loss of the full-scale tail cone. This entrance loss was computed from equation (1). The velocity-pressure term $\frac{\rho V^2}{2g}$ was evaluated from the inlet measurements, and K was taken as 0.23, a widely accepted value for the entrance loss coefficient for a slightly rounded entrance (reference 6). This entrance loss was added to the average inlet total pressure, and the corrected pressure-loss ratio was then $\frac{p'_{av,8} + \Delta p'_{en,8} - p'_{av,9}}{p_9}$. The

value of $p'_{av,9}$ was taken as the average total pressure based on the weight-flow calculations. The Mach number in the discharge duct was computed from pressure in the discharge duct based on the weight-flow calculations and the measured wall static pressure in the discharge duct.

Model air-induction systems. - The evaluation of the pressure-loss ratio and the exit Mach number in the model induction systems also required the determination of the average total pressure in the discharge duct, the static pressure in the discharge duct, and the inlet average total pressure. In the model investigations, the inlet total pressure (room pressure) and the discharge-duct static pressures were measured directly. The average total pressure in the discharge duct for model C was obtained from total-pressure surveys which were made for each run. For models A and B, however, the average total pressure in the discharge duct was known only for two runs and for zero flow condition, where the average pressure is equal to the barometric pressure. For all the runs of all models, the center-line total and wall static pressures in the discharge duct were measured. In order to determine the average total pressure in the discharge duct of models A and B for all the runs, it was necessary to establish the relation between the center-line total pressure and the average total pressure. The center-line total pressure for model C was first plotted. This variation appeared to be linear. The three runs of models A and B for which this variation of average total pressure with center-line total pressure was known were plotted and curves were faired through each set of three points with the variation of model C as a guide. In this manner, the average total pressure in the discharge duct of models A and B was established.



The average total pressure in the discharge duct as determined by the total-pressure surveys was obtained from the following equation:

$$p'_{av,9} = p_9 + \left( \frac{1}{10} \sum_{1}^{10} \sqrt{p'_9 - p_9} \right)^2 \qquad (24)$$

The Mach number in the discharge duct of models A and B was computed from the average total pressure established from the plots of $p'_{av,9}$ against $p'_{\ell,9}$ and the measured static pressure. For model C the measured values of average total pressure and static pressure were used.

## Pressure Losses from Empirical Formulas

The total-pressure losses in the model and full-scale air-induction systems were calculated with loss coefficients readily available in the

[redacted]

literature, in order to obtain a comparison with the measured pressure losses and thus an evaluation of the empirical pressure-loss coefficients and the calculation procedures employed. The general procedure was to start with the measured pressures, weight flow, and total temperature in the discharge duct of the air-induction system and then to calculate upstream in a stepwise manner until the inlet total pressure was established. The discharge conditions of a tail-cone air-induction system are fixed by the pressure requirements of the turbine rotor, and it is necessary for the designer to calculate upstream from this point in order to determine the proper pressure at which to bleed the engine compressor. Consequently, it was thought best to illustrate the calculation procedure in the manner required for design. For the purposes of calculating the pressure losses, the air-induction system was divided into three principal sections. These sections are indicated on figure 6 for each of the three model systems. The detailed pressure-loss calculation procedure for each air-induction system differs in some respects and is therefore discussed separately.



Full-scale tail cone pressure losses. - The pressure losses in the full-scale configuration were computed, starting with the average total pressure and the Mach number in the discharge duct, which were determined by the previously described methods. The Mach number and the measured static pressure were used to establish the velocity pressure by the following formula:

$$\frac{\rho V^2}{2g} = \frac{p\gamma}{2} M^2 \tag{25}$$

The static temperature at the discharge measuring station was then calculated from the discharge Mach number, and the measured effective temperature as the true total temperature at this station. This value of static temperature was used to determine the viscosity $\mu$ from the tables of reference 11. The Reynolds number and friction factor at the exit of the discharge duct were then calculated from equations (4) and (3), respectively. The approximate pressure loss in the discharge duct was computed from equation (2) with all variables as evaluated at the exit of the discharge duct. The approximate total pressure at the inlet to the discharge duct was then obtained by adding the total-pressure loss to the total pressure at exit. This value of total pressure was used to calculate the compressible-flow parameter $\frac{p'A}{w_a\sqrt{gRT}}$, and the charts of reference 10 were used to obtain the static pressure at the inlet to the discharge duct. The Mach number at this point was determined from the total and static pressures. The velocity head and friction factor at the inlet to the discharge duct were calculated in the same way as at the discharge and were averaged with those values calculated at the exit; these average values were used in equation (2) to obtain a refined pressure loss. This process was repeated until the calculated pressure losses agreed within 0.01 inch of mercury.

After the conditions at the inlet to the discharge duct were established, the pressure loss between the exit of the inlet-air tubes and the inlet of the discharge duct was calculated from equation (9). The loss in terms of equivalent feet of straight duct was obtained from reference 6 for a standard T-fitting. The friction factor and velocity pressure were evaluated at the inlet to the discharge duct. The total pressure at the exit of the inlet-air tubes was obtained by adding this loss to the total pressure at the inlet to the discharge duct.

The total-pressure loss in the inlet-air tubes was established in the same manner as was used for the discharge duct. The conditions at the exit were used to establish the values of velocity pressure and friction at this point, and these values were used to determine an approximate total pressure at the entrance to the inlet-air tubes. As before, this total pressure, the weight flow, the total temperature, and the area were used to establish the friction factor and velocity pressure at the tube inlet, which was averaged with the similar values at the discharge of the inlet-air tubes. The process again was repeated until the calculated pressure losses checked within 0.01 inch of mercury. These calculations gave the total-pressure loss between stations 8 and 9 for comparisons with the measured values.

Model A. - The procedure for calculating the pressure loss in model A was similar to the calculations for the full-scale tail cone, except that an entrance loss was computed for the inlet to model A, because the measured loss was from ambient conditions to station 9. This entrance loss was calculated from equation (1), where the value of $K_{en}$ was established as 0.23 from reference 5 for a slightly rounded entrance. This entrance pressure loss was then added to the total pressure at the inlet of the primary-air supply tubes to establish a calculated ambient pressure for the model.

Model B. - The pressure losses in the discharge duct of model B were established in the same manner as the corresponding losses in the full-scale system and model A. The losses in the transition section of model B (see fig. 6) were determined in a stepwise manner. The loss at the entrance to the discharge duct was computed from equation 7, where the value of the loss coefficient $C_c$ in equation (8) was determined from reference 5 for the geometry of model B. The total pressure in the interior of the transition section was obtained by adding this loss to the total pressure at the entrance to the discharge duct.

The pressure loss which occurred at the entrance to the transition section was calculated from equations (5) and (6). The velocity pressure term had to be evaluated in the exit of the inlet section, and because this quantity was not determined until the pressure loss was established, an iteration calculation was necessary. The initial value

of the velocity pressure at the exit of the inlet section $\left(\frac{\rho V^2}{2g}\right)_u$ was established by assuming the velocity pressure to vary only with the area and calculating this quantity from the following equation:

$$\left(\frac{\rho V^2}{2g}\right)_u = \left(\frac{A_d}{A_u}\right)^2 \left(\frac{\rho V^2}{2g}\right)_d \tag{26}$$

where the subscript u refers to the location in the inlet tubes immediately upstream of the transition section, and the subscript d refers to the location immediately downstream of the transition in the discharge duct. With the pressure loss at the entrance to the transition section computed in this manner, the conditions at this position were evaluated and a corrected value of velocity pressure computed. This refined value of velocity pressure was used to obtain a new pressure loss which was checked against the initially calculated pressure loss. This process was repeated until two successively calculated pressure losses agreed within 0.01 inch of mercury.

When the pressure in the exit of the inlet section was established by the final step of the iteration process, the pressure loss in the inlet section and the entrance loss were calculated in the same manner as the corresponding losses of model A.

Model C. - The calculations for the discharge-duct pressure losses were made in the same manner as for the previous configurations. The pressure losses in the transition section (see fig. 6) were calculated from equation (9a). The value of the bend loss coefficient $K_b$ was established from the data of reference 7 for the geometry of model C. Because the data of this reference had to be extrapolated both for Reynolds number range and geometry variables, the accuracy of the value thus established was somewhat uncertain. The calculation, however, was made in this manner in order to test the reliability of such an extrapolation, because, for the geometry ratios which will be probable in tail-cone air-induction systems of this type, the pressure-loss data are very limited, and extrapolations of this type will very likely be required of the designer of a tail-cone air-induction system. The velocity pressure term was evaluated at the entrance to the transition section by an iteration process identical to the one described for the entrance to the transition section of model B. The calculation of the losses in the inlet supply tubes and the entrance correction were made in the same way as the corresponding calculations for models A and B.

Effect of Tail-Cone Pressure Loss on Engine Performance

In order to establish the effects of pressure loss on engine performance, a calculation of engine thrust and specific fuel consumption was made for a centrifugal-flow-type turbojet engine. These performance variables were calculated for an engine with no cooling losses and for engines with pressure losses in the cooling-air-induction systems equal to the pressure losses in models A and C. The calculations were made both for sea-level take-off and for a 50,000-foot altitude at a flight Mach number of 0.8.

The engines for which the thrust and specific fuel consumption were calculated had the following characteristics at both sea level and 50,000 feet:

(1) Engine compressor pressure ratio $p_2'/p_1' = 4.0$

(2) Engine compressor efficiency $\eta_C = 0.76$

(3) Average Mach number relative to the turbine rotor blade $M_4 = 0.54$

(4) Effective gas temperature relative to the turbine rotor blade $(T_{g,e})_4 = 1450^\circ$ F

(5) Turbine-inlet total pressure $p_3' = 0.95\ p_2' = 3.8\ p_1'$

(6) Turbine corrected weight-flow rate $w_g\sqrt{\theta_3}/\delta_3 = 41.0$ lb/sec

(7) Turbine efficiency $\eta_T = 0.80$

(8) Engine speed $N = 11{,}500$ rpm

The turbine efficiency was assumed to be independent of cooling-air flow. These engine conditions are believed to be reasonably characteristic of air-cooled turbojet engines and were largely obtained from operating experience acquired with a nonstrategic, air-cooled engine at the Lewis laboratory. The two cooled-engine configurations of this calculation had air-cooled, nonstrategic, 10-tube, shell-supported turbine-rotor blades with an average temperature at one-third span of 1000° F.

The pressure losses in the bleed system between the compressor bleed point and the inlet to the air-induction system were difficult to estimate accurately, because the geometry of the cooling-air bleed system may depend to a considerable extent on the particular engine installation and on the cooling-air control requirements of the engine.

In order to introduce these pressure losses into the engine performance calculations, the pressure losses in this part of the system arbitrarily were assumed to be equal to those in model A.

Determination of turbine-inlet gas temperature and combustion-gas flow. - The turbine-inlet gas temperature, for all the engine configurations considered, was established in the following manner. The Mach number relative to the rotor $M_4$ was used to establish the total-to-static temperature ratio $T_4'/T_4$. The recovery factor $\Lambda$ for the turbine blade was then determined from the data of reference 8. The static temperature at the turbine rotor was found from a simultaneous solution of the equation of the recovery factor and the equation for total-to-static temperature ratio in terms of Mach number. The static temperature relative to the turbine rotor was assumed to be equal to the static temperature at the discharge of the turbine stator $T_3$. The velocity of the gas leaving the stator was determined from the following expression by assuming the stator discharge Mach number to be 1:

$$V_3 = M_3\sqrt{\gamma_3 g R_3 T_3} \tag{27}$$

The turbine-inlet total temperature $T_3'$ was then calculated from the expression

$$T_3' = T_3 + \frac{V_3^2}{2gJc_{p,3}} \tag{28}$$

The combustion-gas weight flow was then determined from the equation

$$w_g = \frac{41.0\,\delta_3}{\sqrt{\theta_3}} \tag{29}$$

Determination of fuel flow. - The fuel flow for all the engines of these calculations was found by the methods and charts of reference 9. The total temperature at the compressor discharge was calculated from the equation

$$T_2' = T_1'\left[1 + \frac{\left(\frac{p_2'}{p_1'}\right)^{\frac{\gamma_1-1}{\gamma_1}} - 1}{\eta_C}\right] \tag{30}$$

The total temperatures at the compressor outlet and at the turbine inlet were then known, and the fuel-air ratio f was computed from equation (17). A fuel with a lower heating value H of 18,750 Btu per pound



[redacted]

and a hydrogen-carbon ratio of 0.167 and a burner efficiency $\eta_b$ of 0.95 were assumed. Equation (17) was combined with the expression for combustion-gas weight flow

$$w_g = w_A - w_a + w_F \tag{31}$$

to give the fuel flow $w_F$

$$w_F = \frac{f w_g}{1 + f} \tag{32}$$

Determination of cooling-air flow and compressor bleed pressure. - In order to establish first an approximate value of cooling-air flow and compressor bleed pressure, it was assumed that the effective cooling-air temperature at the blade base $T_{e,10}$, the total temperature of the cooling air at the rotor inlet $T'_9$, and the total temperature at the compressor bleed point $T'_7$ were all equal. If an initial value for all these temperatures was assumed, the coolant-flow ratio $w_a/w_g$ could be established as was indicated by equation (15). The heat-transfer characteristics of the 10-tube shell-supported blade presented in reference 12 were used to establish $w_a/w_g$ for the engine conditions at $T_B$ of 1000° F and $(T_{g,e})_4$ of 1450° F. From the previously determined value of the combustion-gas flow $w_g$, the cooling-air flow was established for the assumed temperatures. When the total pressure of the cooling air at the rotor hub and the area of the discharge duct of the air-induction system were assumed, the Mach number and static pressure at this point were determined by the previously described methods. The area of the discharge duct was assumed to be equal to the area of the full-scale air-induction system. The value assumed for the total pressure at the inlet of the turbine rotor was checked later in the calculation when the value of tail-pipe total pressure was established. The turbine rotor was assumed to be capable of delivering a pressure ratio of about 1.0, and the assumed value of total pressure at the rotor hub was thus required to be equal to the turbine-discharge total pressure. The cooling-air conditions at the rotor hub permitted the evaluation of the pressure losses through models A and C from the data presented with this report. The compressor bleed pressure was then calculated from

$$p'_7 = p'_9 + (\Delta p')_{7-8} + \Delta p'_{8-9} \tag{33}$$

In this investigation the total-pressure loss between stations 7 and 8 is not known. However, in order to include some pressure loss for this section of the ducting system in the engine performance calculations, the pressure loss was arbitrarily assumed to be equal to that through the tail-cone ducting system of model A. Equation (33) therefore can be written for model A as

[redacted]

$$(p_7')_{\text{model A}} = p_9' + (2\Delta p_{8-9}')_{\text{model A}} \tag{33a}$$

and for model C

$$(p_7')_{\text{model C}} = p_9' + (\Delta p_{8-9}')_{\text{model C}} + (\Delta p_{8-9}')_{\text{model A}} \tag{33b}$$



The initially assumed temperature at the compressor bleed point was then checked by the equation

$$T_7' = T_1'\left[1 + \frac{\left(\frac{p_7'}{p_1'}\right)^{\frac{\gamma_1-1}{\gamma_1}} - 1}{\eta_C}\right] \tag{34}$$

This calculation was repeated until the initially assumed temperatures in the cooling-air system agreed with the calculated value within 1° F in order to establish the approximate values of cooling-air flow and bleed pressure. These approximate weight flows were then used with the data of reference 3 to determine the temperature rise of the cooling air in the tail cone and in the interior of the air-cooled turbine rotor between the rotor inlet and the base of the cooled turbine blades. With these temperature increases established, a new temperature of the cooling air at the blade base was assumed and the calculation repeated, with the temperature increases established by the initial calculation and more refined values of the cooling-air flows and compressor bleed pressure considered.

Determination of engine thrust and specific fuel consumption. - The specific turbine work $\Omega$ was calculated from equation (18), and the total temperature and total pressure downstream of the turbine were obtained from the following rearrangement of equations (19) and (20), respectively:

$$T_5' = \frac{c_{p,3}\,T_3' - \Omega}{c_{p,3}} \tag{19a}$$

and

$$p_5' = p_3'\left(1 - \frac{\Omega}{\eta_T c_{p,3}\,T_3'}\right)^{\frac{\gamma_3}{\gamma_3-1}} \tag{20a}$$

The jet velocity $V_6$ was determined from equation (21), and the engine thrust and specific fuel consumption from equations (22) and (23), respectively.

## RESULTS AND DISCUSSION

### Flow Characteristics

The total-pressure distribution in the discharge ducts of all the air-induction configurations was measured in order to establish the character of the cooling-air flow in the discharge duct.

Total-pressure profiles in model air-induction systems. - The behavior of the cooling-air flow in the discharge duct of the model configurations was determined by a total-pressure survey taken at the maximum weight-flow condition for each model. The total-pressure profiles would be similar at lower weight flows, but the variation in total pressure across the duct would be less pronounced. The results of these surveys are shown in figure 7.

For model A the total pressure rose sharply near the walls and reached a maximum value at points equivalent to about 10 and 90 percent of the discharge-duct diameter. This maximum value of total pressure remained essentially unchanged for about the next 10 percent of the diameter toward the center of the duct and then showed a slight decrease near the center. This decrease indicates that a slight vortex may be present in the discharge duct of model A; however, the vortex was not considered to be appreciable, and no attempt was made to eliminate it.

The total-pressure profiles of model B are shown for model B without and with straightening vanes in the discharge duct. Without straightening vanes the total pressure is low in the center portion of the duct and relatively high near the walls. This type profile indicates that a strong vortex exists in the duct. The total pressures were obtained with the total-pressure probe pointed in an axial direction; consequently, only the axial component of the total pressure is recorded, and the kinetic energy of the vortex is not indicated. The cause of the vortex is not definitely known, but a slight degree of misalinement of the inlet-air tubes or some other lack of symmetry in the model configuration may have caused the initial formation of the vortex in the transition section of model B, and the convergence of the air flow as it enters the discharge duct probably acted to increase the intensity of the vorticity.

The presence of a strong vortex in the discharge duct is not desirable, because accurate flow measurements in the duct would be difficult to obtain, and the vortex would also contribute to high pressure losses. In an attempt to eliminate the vortex in the discharge duct, a set of four axial straightening vanes equal in length to 1.5 discharge-duct diameters was placed at the entrance to the discharge duct. The effectiveness of the straightening vanes in eliminating the vortex in the discharge duct can be seen in figure 7 by comparing the total-pressure

profile with straightening vanes to the profile previously obtained without the vanes. With the straightening vanes, variation in total pressure throughout about 90 percent of the discharge-duct diameter was relatively small. Hereinafter, all data presented for model B are for the case with straightening vanes.



The total-pressure profile of model C was relatively uniform across the discharge duct. A slight increase in total pressure near one wall (at about 70 percent of the duct diameter) may have been caused by a slight difference in weight flows through the two eliptical inlet-air tubes.

Comparison of measured center-line total pressure with average total pressure in discharge ducts of full-scale and model tail cones. - The relation between the center-line total pressure and the calculated average total pressure in the discharge duct of the full-scale tail cone is shown in figure 8. Data for both a restricted and an unrestricted outlet are shown. The data indicate that for the range of total pressures investigated there is a linear relation between the center-line total pressure and the calculated average total pressure for the runs with a restricted outlet. For the unrestricted outlet there is also a linear relation except for the total pressure between about 30 to 34 inches of mercury.

The relation between the measured center-line total pressure and the measured average total pressure in the discharge duct for the three scale-model tail cones is shown in figure 9. Because no measurements of the weight flow were made during the model tests, the average total pressure was determined only from pressure surveys made in the discharge duct. Total-pressure surveys in the discharge duct were made for all the runs of model C and for only three runs for models A and B. The variation between the center-line total pressure was linear for all the models as shown in figure 9. Although only three data points were obtained for models A and B, the linear relation between the center-line total pressure and average total pressure in the discharge duct is substantiated by the more numerous data obtained for the full-scale tail cone (fig. 8) and for model C in figure 9. Because no total-pressure survey data for models A and B were obtained between center-line total pressures of about 22 and 29.5 inches of mercury, the average total pressure in the discharge duct for these models was determined by the center-line total-pressure measurement and the use of figure 9.

Figure 9 also indicates that for model A the average total pressure is higher than the center-line total pressure, which can be explained by referring to figure 7, where for model A the value of the center-line total pressure is lower than for any point in the duct, possibly as a result of secondary flows except in the region of the duct walls. For models B (with straightening vanes) and C, figure 9 shows that the

average total pressure is equal to the center-line total pressure. The total-pressure profiles in figure 7 for models B (with straightening vanes) and C indicate that this relation might be expected.



## Measured Total-Pressure Losses

Model tail-cone air-induction systems. - The total-pressure loss through the model cooling-air-induction systems was presented by a pressure-loss ratio $\frac{p'_{am} - p'_{av,9}}{p_9}$, which was plotted against the Mach number in the discharge duct. Figure 10 shows the relation between the pressure-loss ratio and Mach number for models A, B, and C. The superiority of model C with respect to pressure loss is readily apparent, the values of pressure-loss ratio for models A and B being about 300 and 400 percent greater, respectively, than those for model C. The values obtained with model C indicate that a considerable reduction in pressure loss through the ducting system can be effected by a careful design of the system. The low pressure losses of model C in comparison with those of the other models would be expected from an inspection of the geometry of the models (fig. 2). In model C the cooling air was smoothly turned through 90° by each of the two inlet-air supply tubes and was then directed axially into the discharge duct by each tube. In models A and B the turning of the air was abrupt, and direct interference between the air streams leaving the primary-air inlet tubes no doubt contributed to the over-all total-pressure losses. Furthermore, in model B the sudden expansion of the cooling air as it entered the transition section and the sudden contraction as the air entered the discharge duct also contributed to the pressure losses of this model. Also the presence of a vortex in model B, as discussed previously, would result in additional pressure losses. The use of straightening vanes in the discharge duct of model B probably helped to reduce some of the pressure losses associated with a high vortex, but considerable loss of total pressure due to high angle of incidence at the entrance to the straightening vanes probably existed. It is believed that the straightening vanes of model B served mainly as a method of smoothing the flow in the discharge duct and thus provided more reliable pressure measurements in the duct.

Full-scale tail cone. - The relation between the pressure-loss ratio and the discharge-duct Mach number for the full-scale tail cone is shown in figure 11 for both a restricted and an unrestricted outlet. For the full-scale tail cone there appears to be a definite pressure-level effect, highest pressure-loss ratios being associated with the highest pressure levels. The separation of the curves for the restricted and the unrestricted outlet runs may be a result of differences in the density variation in the two sets of runs. The outlet static pressure used in the pressure-ratio parameter may bear, at a given Mach number, a different relation to the average static pressure of the system for each set of

runs. As a result, the two sets of data are effectively being referred to different densities, and some separation of the curves would be expected.

Figure 11 indicates that the pressure-loss ratios for model A, which are included for comparison, are less than for the full-scale tail cone. This separation may be due to a pressure-level difference between the model and the full-scale configuration, rather than to a scale effect. The data for the full-scale tail cone have been corrected for the differences in the lengths of the inlet and outlet ducts between the full-scale configuration and model A.



## Comparison of Calculated and Measured Total-Pressure Losses

The comparison of calculated and measured over-all total-pressure losses presented in figure 12 indicates the reliability of the loss coefficients and calculation procedures employed.

Model A. - The calculated pressure losses through model A were about 40 percent less than the measured values over most of the range of this investigation. This discrepancy was probably due largely to unreliable values of the loss coefficients used to determine the losses in the transition section of the model.

Model B. - The calculated pressure losses in model B showed the largest variation from the measured losses, being about 65 percent less, probably because of the existence of a vortex flow in the transition section which was not accounted for by the calculations. Also, because of the nonaxial direction of the air as it entered the discharge duct and the straightening vanes, there may have been considerable flow separation on the upstream end of the straightening vanes which resulted in a throttling effect far in excess of the contraction loss assumed in the calculations.

Model C. - The calculated losses for model C appear to agree reasonably well with the measured values, averaging about 12 percent lower. This discrepancy was probably caused by an inaccuracy in the loss coefficient for the 90° bend of the elliptical inlet ducts. The duct system of model C is the least complicated with respect to flow, and it might be expected that the pressure losses for this model could be calculated more accurately than the losses of models A and B. Because of the low Reynolds numbers and unusual geometry encountered in these model tests, the data available sometimes had to be extrapolated both for Reynolds number range and geometry variables. In this low Reynolds number range the data of reference 7 indicate that such extrapolations are questionable.

The problem of the variation of loss coefficients with Reynolds number in the low Reynolds number range indicated by the literature may be encountered by the designer of a full-scale tail-cone air-induction system at the altitude design point. The uncertainties involved in the proper selection of the loss coefficients indicate that the pressure-loss design of the bleed system should be conservative in order to satisfy the pressure requirements of the turbine rotor.



### Effect of Tail-Cone Pressure Loss on Engine Performance

The results of the engine performance calculations are presented in table I. The losses in the tail-cone air-induction systems were taken as equal to the losses through models A and C as explained in the CALCULATION PROCEDURE section. The assumptions that the turbine stator remained choked and that the turbine-inlet temperature remained constant resulted in a higher compressor mass flow for the cooled engines than for the uncooled engine. The characteristics of a centrifugal-flow compressor are such that these changes in weight flow could probably be accomplished at a constant pressure ratio without a change in the frontal area of the engine. For an axial-flow engine, however, these changes in compressor air flow would require changes in the compressor-inlet area, and as a result the cooled axial-flow engines would have a larger frontal area than the uncooled engine.

The engine performance losses associated with the differences in bleed-system pressure losses between systems A and C were negligible both at sea level and 50,000 feet. The differences in performance between the cooled engines and the uncooled engine were small. As a result, it appears that for present-day engines requiring coolant-flow ratios of about 2 to 4 percent, the engine performance losses associated with the bleed-system pressure loss is negligible, and considerable aerodynamic refinement of the cooling-air bleed system is not necessary unless the pressure requirements of the cooled turbine rotor cannot otherwise be met by the engine compressor.

### General Recommendations for Tail-Cone Cooling-Air-Induction-System Design

The generally accepted procedure for designing low pressure-loss ducting systems should be employed in the design of a cooling-air-induction system for an air-cooled turbine rotor. The mechanical simplicity of the system, however, need not be appreciably sacrificed unless it is necessary to meet the pressure requirements of the turbine rotor. The effect of the bleed-system pressure losses on engine performance does not appear to be sufficient to warrant any considerable complication of the air-induction system, provided the cooling-air requirements of the engine are small (2 to 4 percent) compared with the turbine gas flow.

Large chambers should be avoided. They may develop intense secondary flows (vortex of model B) which will contribute unnecessarily to the pressure losses in the cooling-air system.

The apparent variation in some loss coefficients in the low Reynolds number range (below $2 \times 10^5$) with Reynolds number indicates that the altitude pressure-loss design of the air-induction system should be conservative in order to ensure that the pressure-loss requirements of the turbine rotor will be fulfilled.



## SUMMARY OF RESULTS

The important results of this tail-cone air-induction-system investigation can be summarized as follows:

1. For the three model tail cones investigated, the pressure-loss ratios of model C were the lowest, those for models A and B being about 300 and 400 percent higher, respectively, than those for model C.

2. There appeared to be a high degree of vorticity in model B which contributed to the high pressure losses through this configuration.

3. The calculated total-pressure losses through the model systems were lower than the measured values, probably generally because of the use of incorrect loss coefficients. Because of the limited data on loss coefficients at low Reynolds numbers, the altitude design of the bleed system should be conservative in order that the pressure requirements of the cooled turbine rotor can be satisfied.

4. The effect of tail-cone pressure losses on the engine performance variables, thrust and specific fuel consumption, were found to be negligible for air-cooled engines operating with coolant-flow ratios of about 2 to 4 percent. This result is in agreement with previously calculated results. A great deal of aerodynamic refinement of the cooling-air-induction system does not appear to be justified unless it is required to fulfill the pressure requirements of the turbine rotor, in which case considerable improvement in pressure-loss characteristics of the bleed system can be obtained with some sacrifice in mechanical simplicity, as is indicated by the superiority of model C to models A and B.

Lewis Flight Propulsion Laboratory
National Advisory Committee for Aeronautics
Cleveland, Ohio

[redacted]

## APPENDIX - SYMBOLS

The following symbols are used in this report:

A cross-sectional area, sq ft

C constant

$c_p$ specific heat at constant pressure, Btu/(lb)(°F)

d hydraulic diameter, ft

F thrust, lb

f friction factor $\left(f = \frac{d}{l} \frac{\Delta p' 2g}{\rho V^2}\right)$, or fuel-air ratio $\left(f = \frac{W_F}{W_A - W_a}\right)$

g ratio of absolute to gravitational unit of mass, lb/slug, or acceleration due to gravity, ft/sec$^2$

H lower heating value of fuel at 600° R, Btu/lb

h enthalpy $\left(\int_{600^\circ R}^{T} c_p \, dt + 48\right)$, Btu/lb

h' enthalpy based on total temperature, Btu/lb

J mechanical equivalent of heat, 778 ft-lb/Btu

K loss coefficient $\left(K = \frac{\Delta p' 2g}{\rho V^2}\right)$

$l$ length, ft

M Mach number

p static pressure, lb/sq ft abs

p' total pressure, lb/sq ft abs

R gas constant

Re Reynolds number

r turbine tip radius, ft

sfc specific fuel consumption

| | |
|---|---|
| T | static temperature, $^{\circ}R$ |
| T' | total temperature, $^{\circ}R$ |
| V | velocity, ft/sec |
| w | weight flow, lb/sec |
| $\gamma$ | ratio of specific heat at constant pressure to specific heat at constant volume |
| $\Delta$ | change as indicated by variable and subscripts |
| $\delta$ | ratio of total pressure to standard NACA sea-level pressure (p'/2116) |
| $\eta$ | efficiency |
| $\theta$ | ratio of total temperature to standard NACA sea-level temperature (T'/518.4) |
| $\Lambda$ | recovery factor, $\frac{T' - T_e}{T' - T}$ |
| $\mu$ | viscosity, lb/(sec)(sq ft) |
| $\xi^I$, $\xi^{II}$ | function of |
| $\rho$ | specific weight, lb/cu ft |
| $\varphi$ | temperature-difference ratio, $\frac{T_{g,e} - T_B}{T_{g,e} - T_{e,10}}$ |
| $\psi_h$ | $\frac{(h'-h'_0)(1+f)}{f}$ (reference 8) |
| $\Omega$ | specific turbine work, Btu/lb |
| $\omega$ | angular velocity, radians/sec |

Subscripts:

| | |
|---|---|
| A | compressor-inlet air |
| a | cooling air |
| am | ambient |

[redacted]

| | |
|---|---|
| av | average |
| B | blade |
| b | bend or burner |
| C | compressor |
| c | contraction |
| $\mathfrak{C}_L$ | center line |
| d | downstream |
| e | effective |
| en | entrance |
| eq | equivalent |
| ex | expansion |
| F | fuel |
| f | friction losses |
| g | combustion gas |
| o | over-all |
| r | reference station in duct system |
| s | secondary flow losses |
| T | turbine |
| u | upstream |
| x | any duct element of length x |
| 0,1,2,3, 4,5,6,7, 8,9,10 | refer to stations in tail-cone system as indicated in figure 5, except when subscript 0 is used with h; it then refers to dry air, zero fuel-air ratio. |

[redacted]

REFERENCES

1. Kemp, Richard H., and Moseson, Merland L.: Investigations of Air-Cooled Turbine Rotors for Turbojet Engines. II - Mechanical Design, Stress Analysis, and Burst Test of Modified J33 Split-Disk Rotor. NACA RM E51J03, 1952.

2. Schramm, Wilson B., and Ziemer, Robert R.: Investigations of Air-Cooled Turbine Rotors for Turbojet Engines. I - Experimental Disk Temperature Distribution in Modified J33 Split-Disk Rotor at Speeds up to 6000 RPM. NACA RM E51I11, 1952.

3. Nachtigall, Alfred J., Zalabak, Charles F., and Ziemer, Robert R.: Investigations of Air-Cooled Turbine Rotors for Turbojet Engines. III - Experimental Cooling-Air Impeller Performance and Turbine Rotor Temperatures in Modified J33 Split-Disk Rotor up to Speeds of 10,000 RPM. NACA RM E52C12, 1952.

4. Arne, Vernon L., and Nachtigall, Alfred J.: Calculated Effects of Turbine Rotor-Blade Cooling-Air Flow, Altitude, and Compressor Bleed Point On Performance Of a Turbojet Engine. NACA RM E51E24, 1951.

5. Dodge, Russell A., and Thompson, Milton J. E.: Fluid Mechanics. McGraw-Hill Book Co., Inc., 1937.

6. Anon.: Flow of Fluids Through Valves, Fittings, and Pipe. Tech. Paper No. 409, Eng. and Res. Div., Crane Co., May 1942.

7. Weske, John R.: Pressure Loss in Ducts with Compound Elbows. NACA ARR Feb. 1943.

8. Ellerbrock, Herman H., Jr., and Stepka, Francis S.: Experimental Investigation of Air-Cooled Turbine Blades in Turbojet Engine. I - Rotor Blades with 10 Tubes in Cooling-Air Passages. NACA RM E50I04, 1950.

9. English, Robert E., and Wachtl, William W.: Charts of Thermodynamic Properties of Air and Combustion Products from 300° to 3500° R. NACA TN 2071, 1950.

10. Turner, L. Richard, Addie, Albert N., and Zimmerman, Richard H.: Charts for the Analysis of One-Dimensional Steady Compressible Flow. NACA TN 1419, 1948.

11. Keenan, Joseph H., and Kaye, Joseph: Thermodynamic Properties of Air. John Wiley & Sons, Inc., 1945.



[redacted]

12. Cochran, Reeves P., Stepka, Francis S., and Krasner, Morton H.: Experimental Investigation of Air-Cooled Turbine Blades in Turbojet Engine. XI - Internal-Strut-Supported Rotor Blade. NACA RM E52C21, 1952.



[redacted]

TABLE I - COMPARISON OF ENGINE PERFORMANCE CHARACTERISTICS FOR SEVERAL BLEED-SYSTEM CONFIGURATIONS

NACA

| Tail-cone configuration | Compressor weight flow $w_A$ (lb/sec) | Cooling-air weight flow $w_a$ (lb/sec) | Cooling-air bleed pressure $p_j$ (in. Hg abs) | Engine specific thrust $F/w_A$ | Specific fuel consumption sfc (lb/hr)/lb |
|---|---|---|---|---|---|
| Sea level | | | | | |
| A | 77.58 | 2.08 | 64.48 | 57.14 | 1.26 |
| C | 77.52 | 2.02 | 58.98 | 57.28 | 1.26 |
| Uncooled | 75.50 | ---- | ----- | 58.70 | 1.26 |
| 50,000 feet | | | | | |
| A | 12.18 | 0.284 | 9.41 | 11.72 | 0.97 |
| C | 12.18 | .280 | 8.83 | 11.73 | .97 |
| Uncooled | 11.90 | ----- | ----- | 11.90 | .98 |

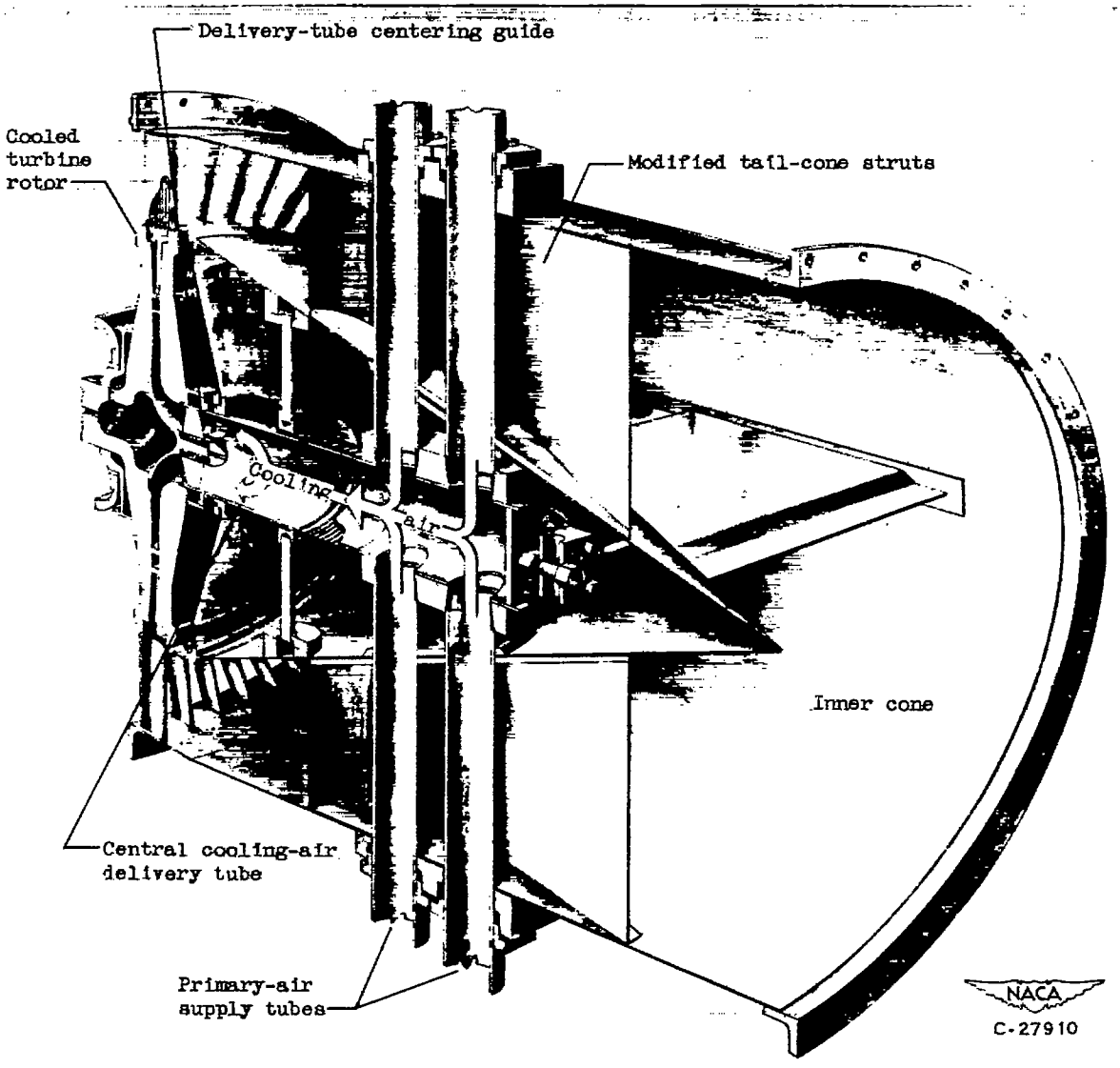


Figure 1. - Sectional view of full-scale tail-cone cooling-air-induction configuration and cooled turbine rotor.

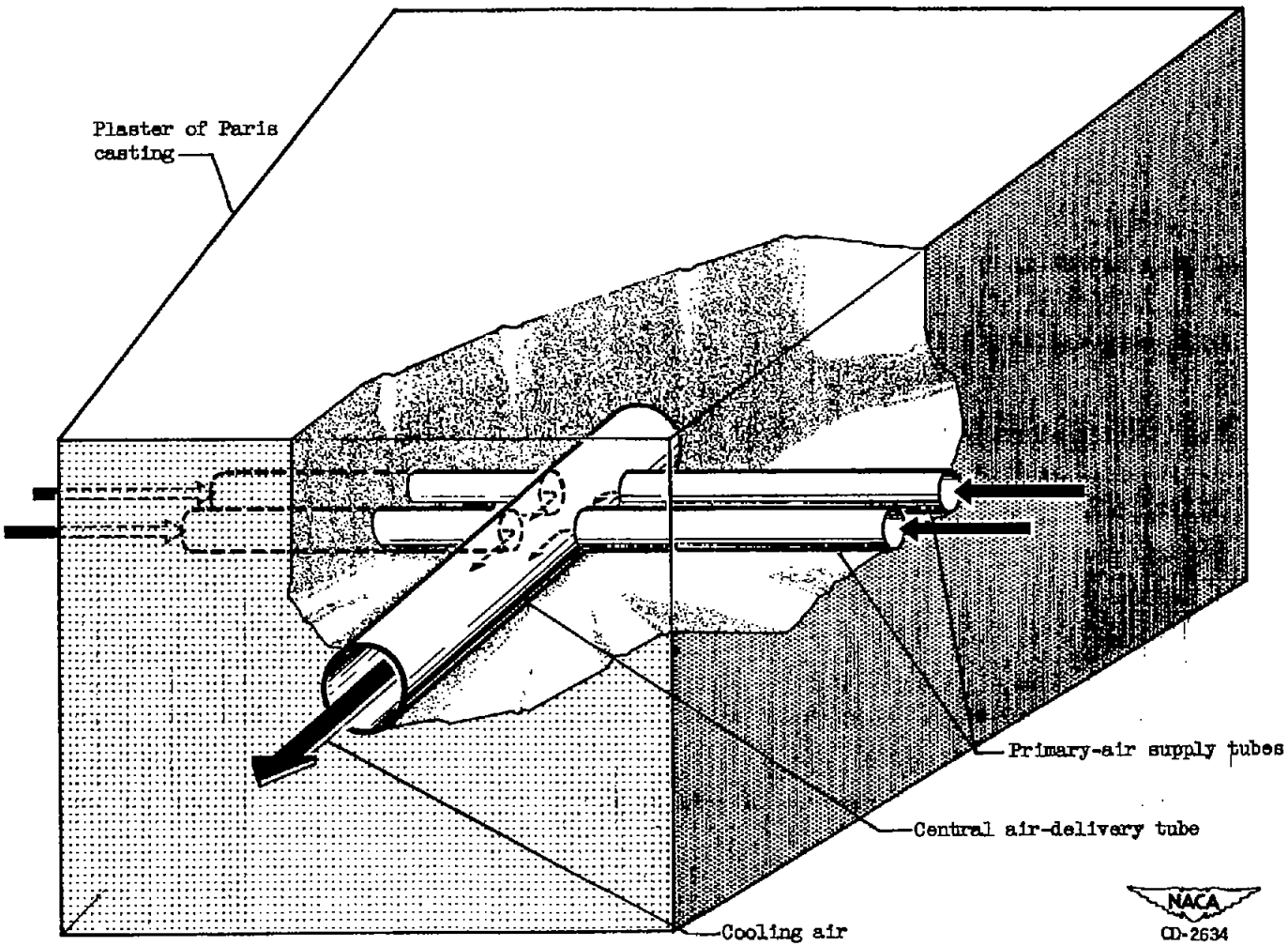


(a) Model A.

Figure 2. - Tail-cone cooling-air-induction-system configurations.

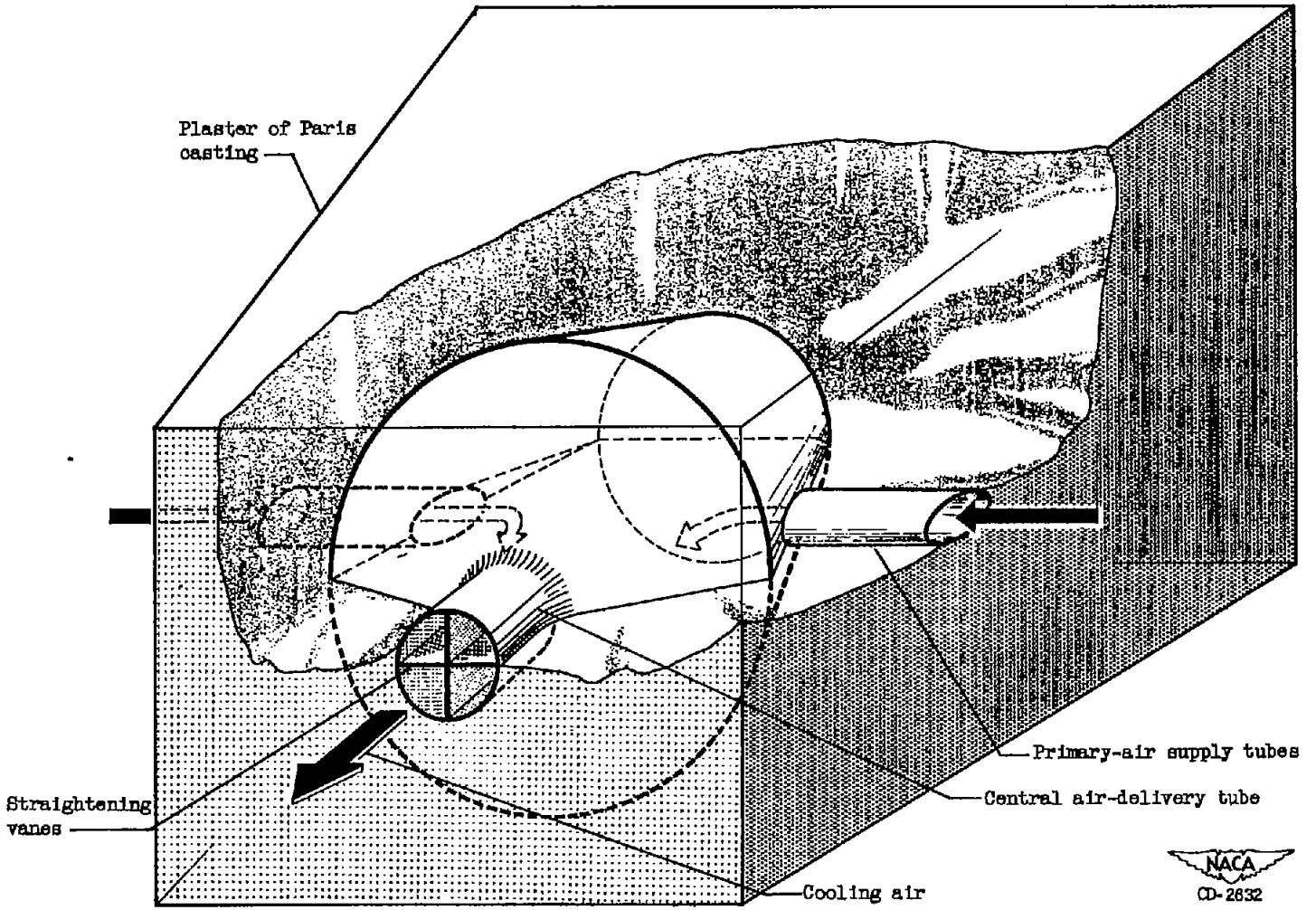


(b) Model B with straightening vanes.

Figure 2. - Continued. Tail-cone cooling-air-induction-system configurations.

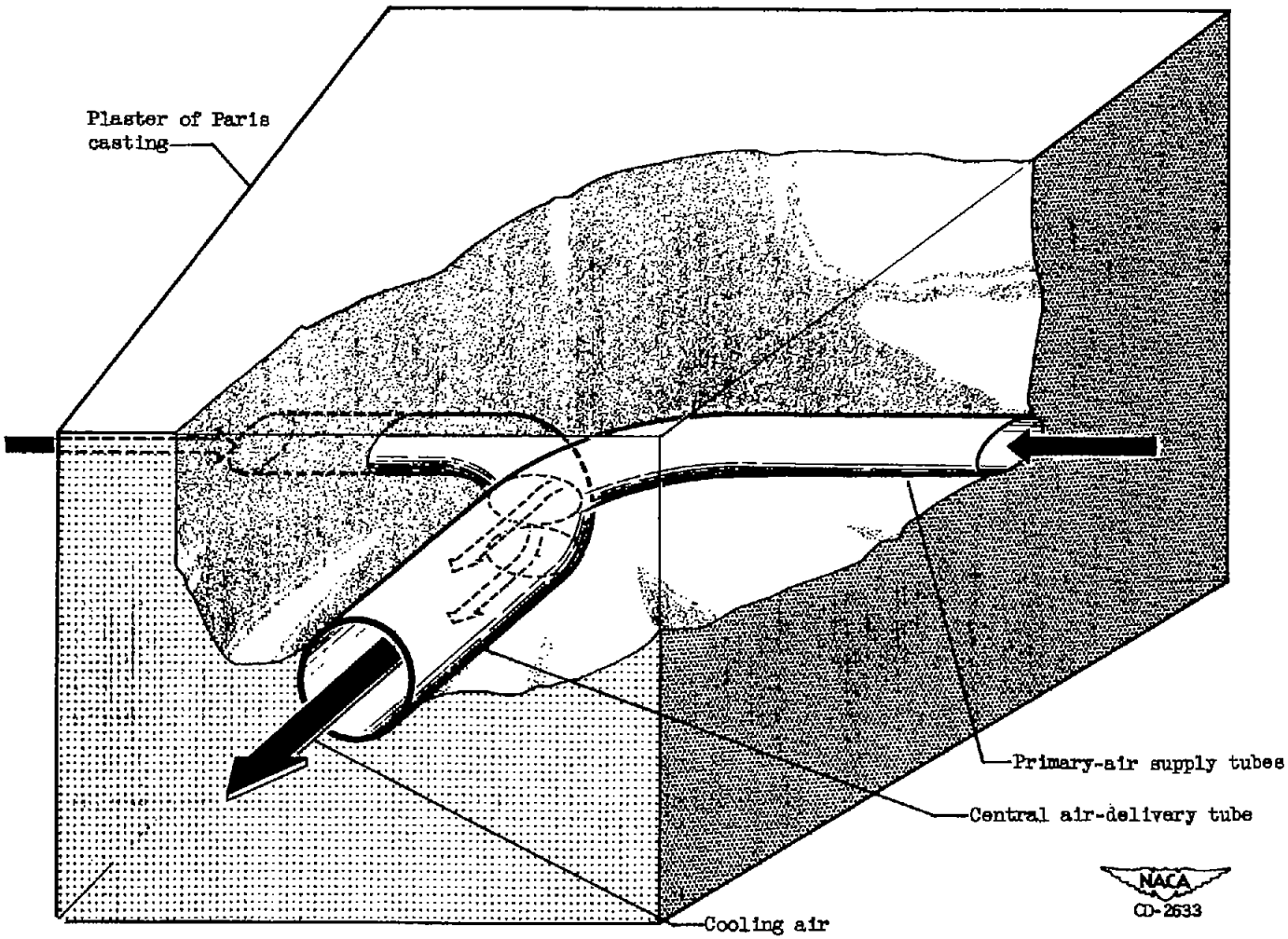


(c) Model C

Figure 2. - Concluded. Tail-cone cooling-air-induction-system configurations.

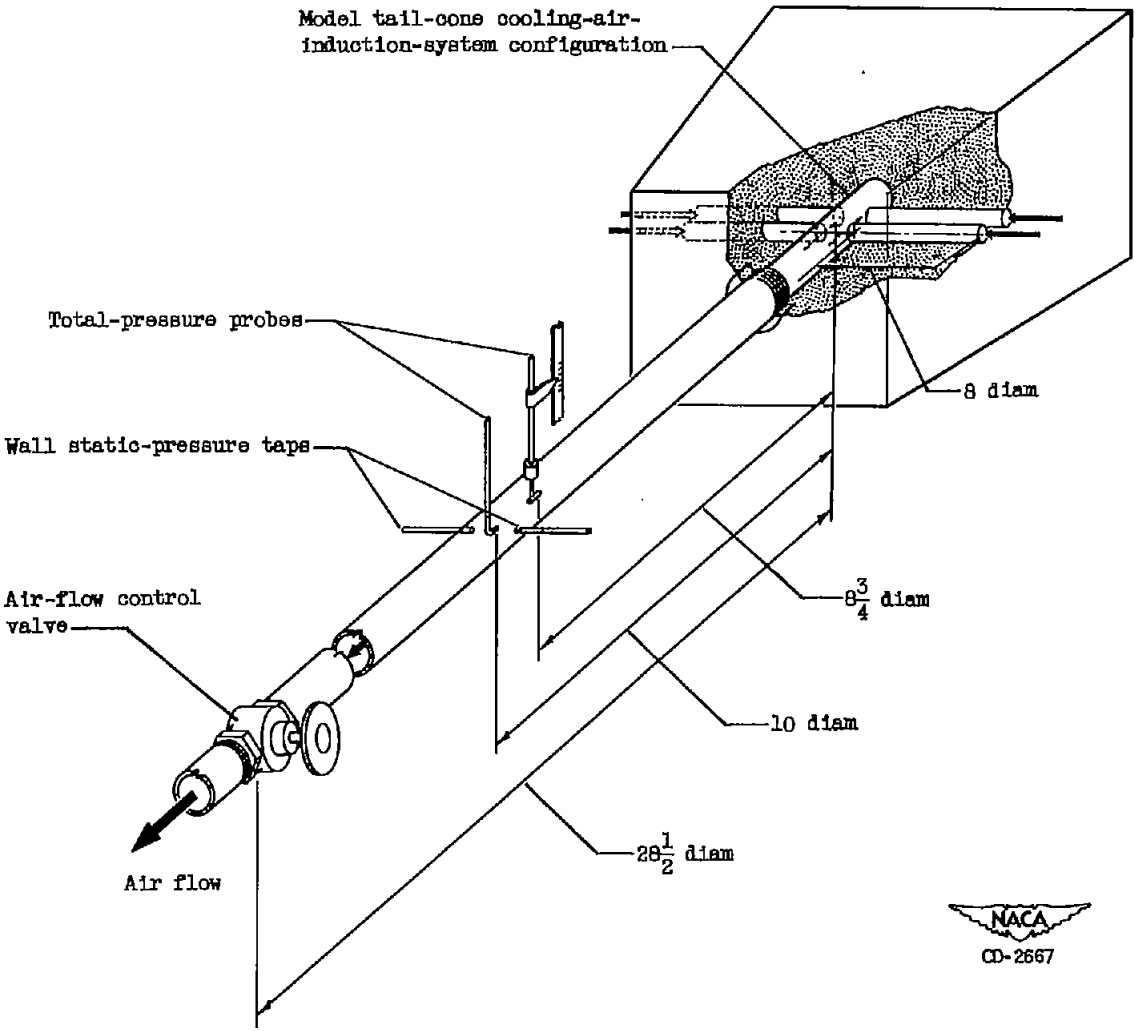


Figure 3. - Schematic diagram of model test installation showing model A in position.

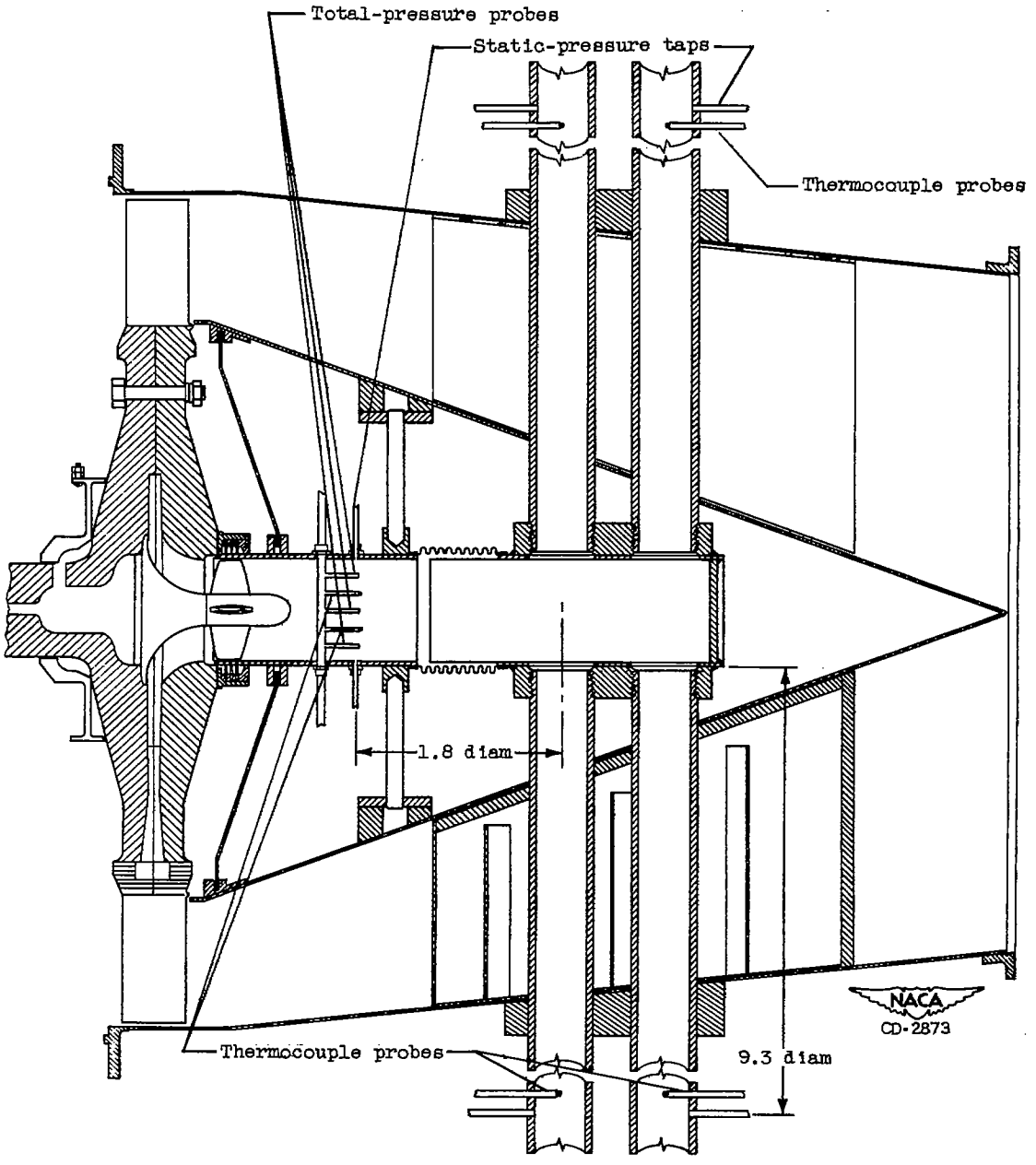


Figure 4. - Instrumentation of full-scale tail-cone cooling-air-induction-system configuration.

[redacted]

Figure 5. - Schematic diagram of engine stations used in subscript notation.

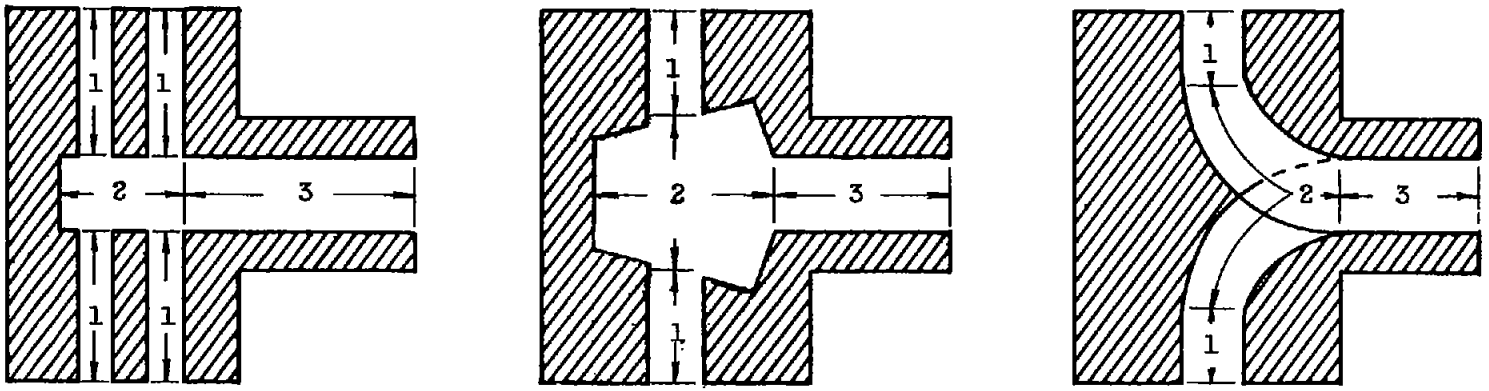


1 Inlet section
2 Transition section
3 Discharge duct

NACA

Figure 6. - Schematic illustration of model tail-cone air-induction configurations A, B, and C.

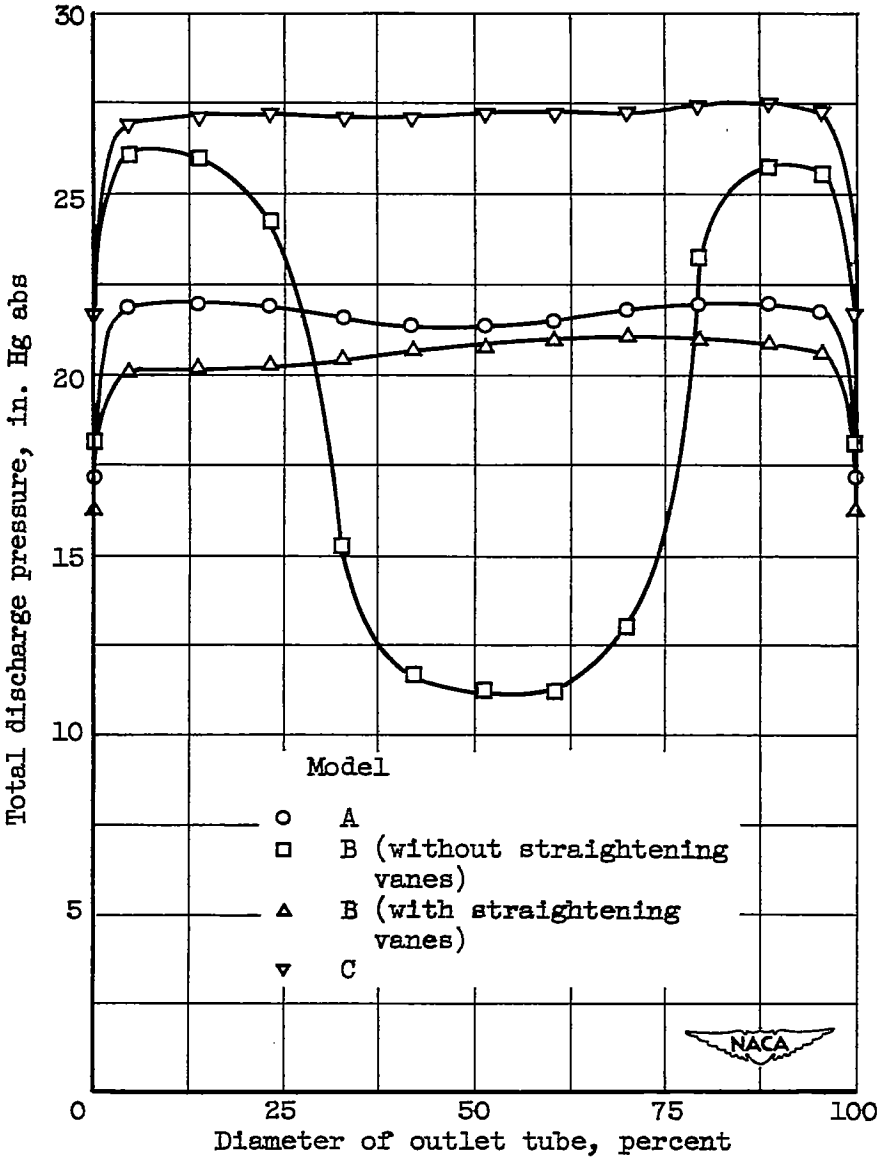


Figure 7. - Comparison of discharge total-pressure profiles for several model cooling-air-induction configurations at maximum mass-flow conditions.

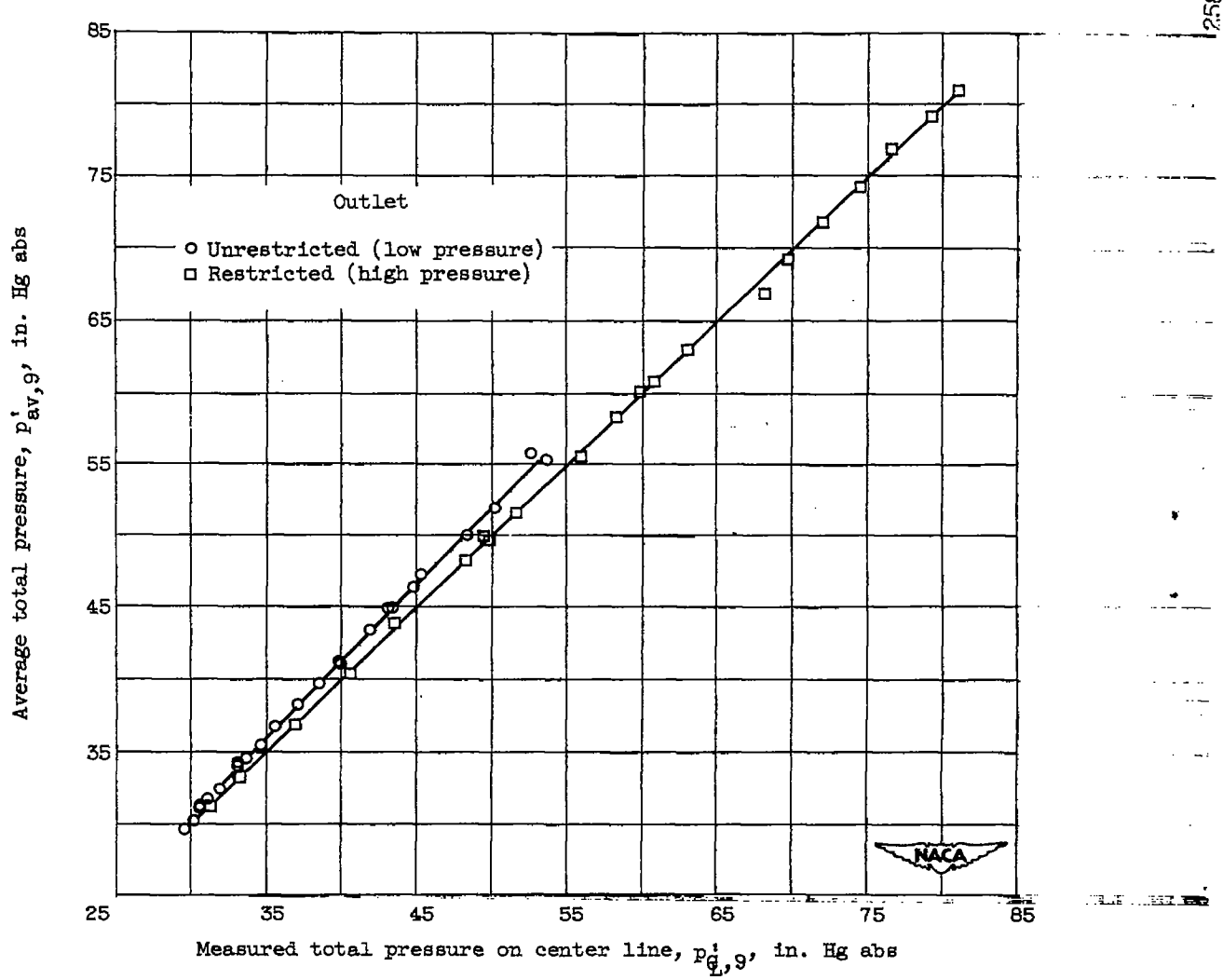


Figure 8. - Comparison of calculated and measured downstream average total pressure for full-scale air-induction system over range of measured center-line total pressures.

[redacted]

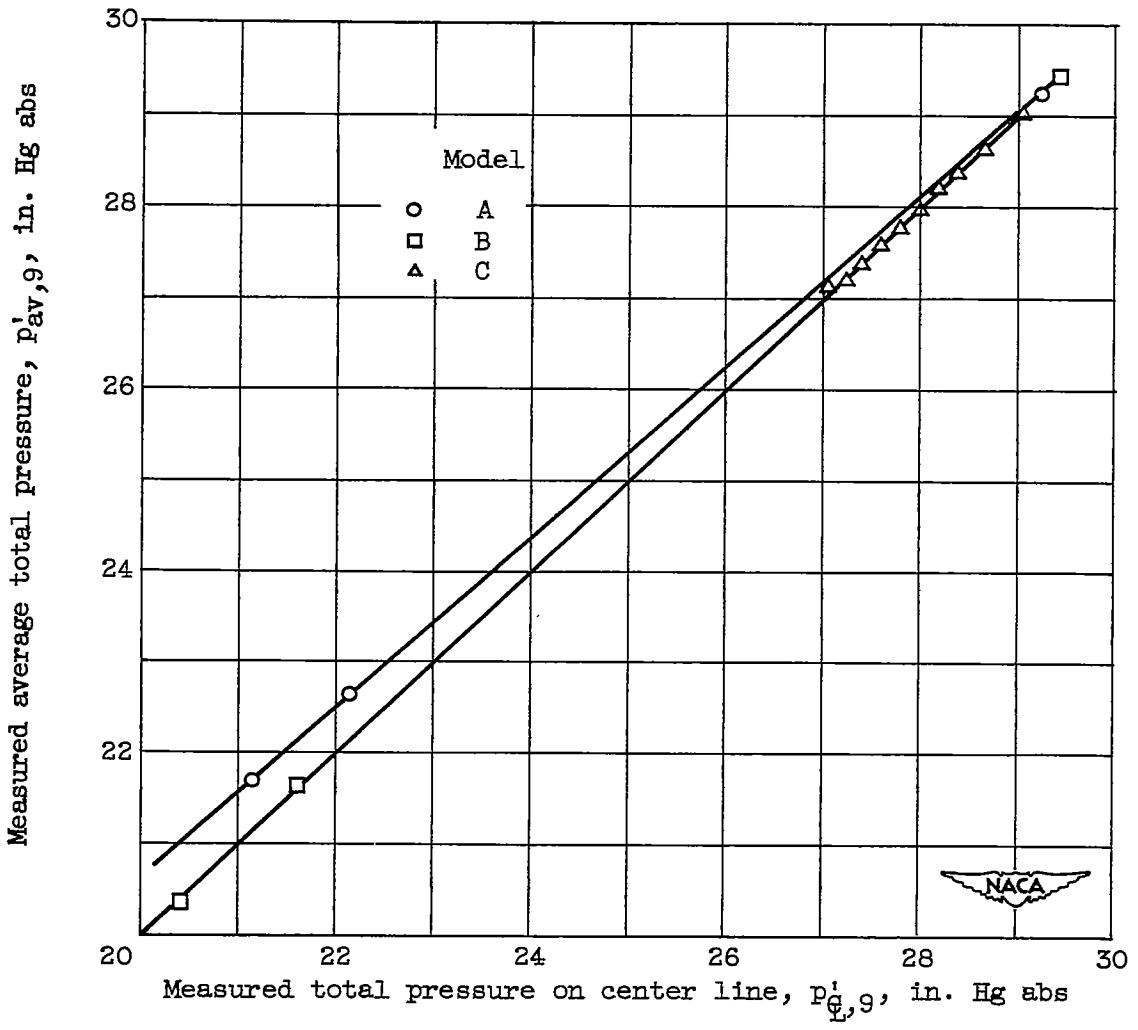


Figure 9. - Comparison of measured center-line and measured average total pressures in discharge tube for model air-induction systems.

[redacted]

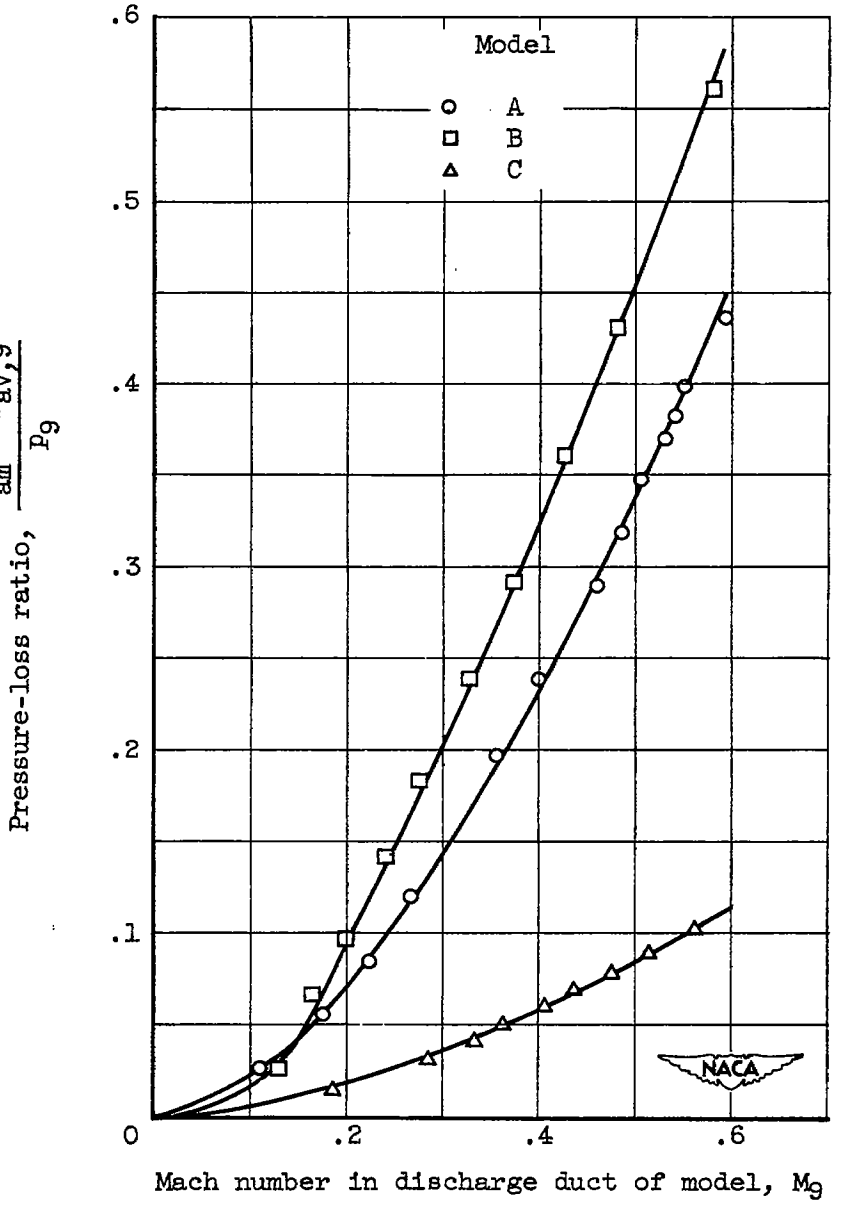


Figure 10. - Comparison of measured over-all pressure losses of model air-induction systems.

[redacted]

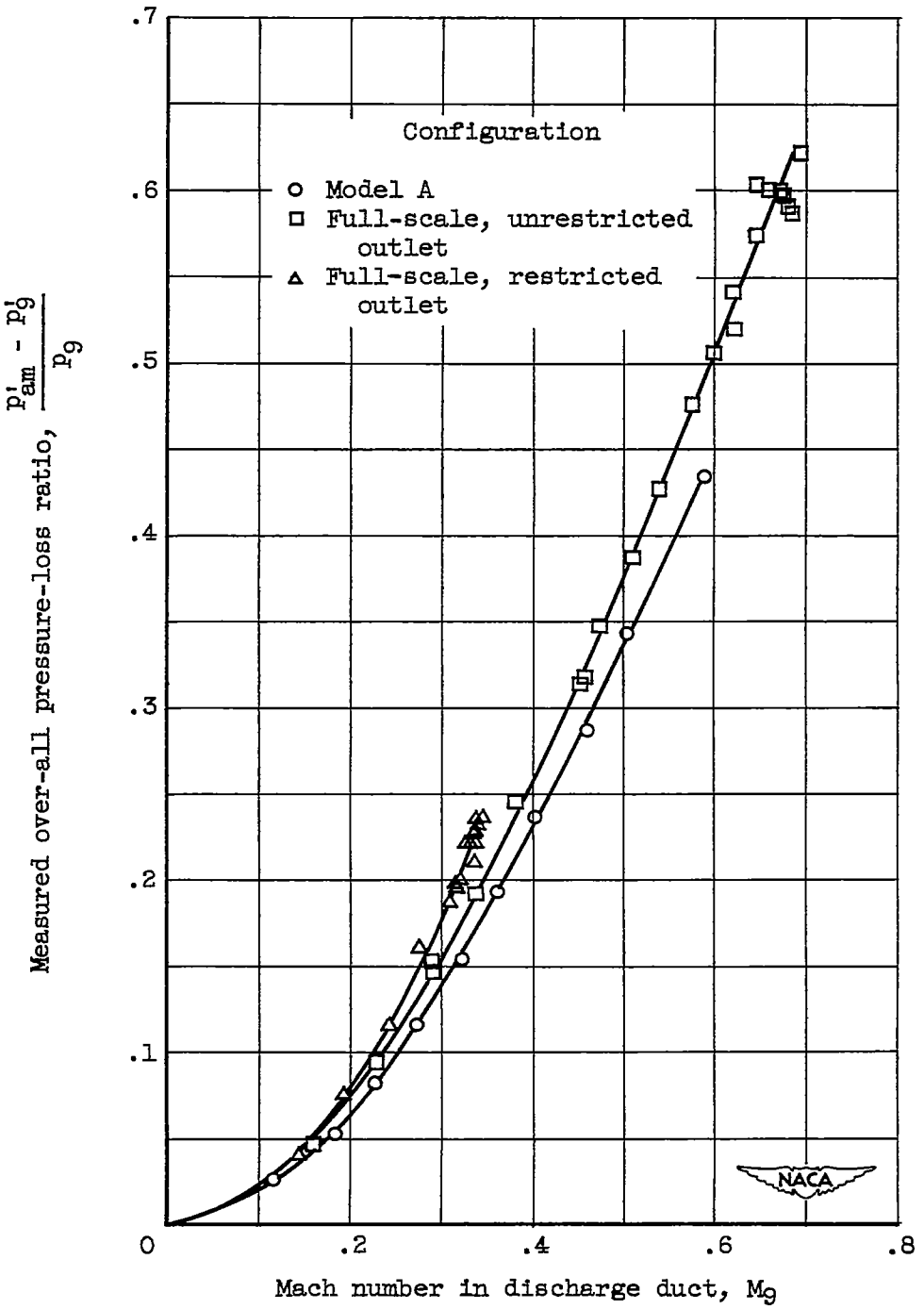


Figure 11. - Comparison of measured over-all pressure losses of model A and similar full-scale air-induction systems.

[redacted]

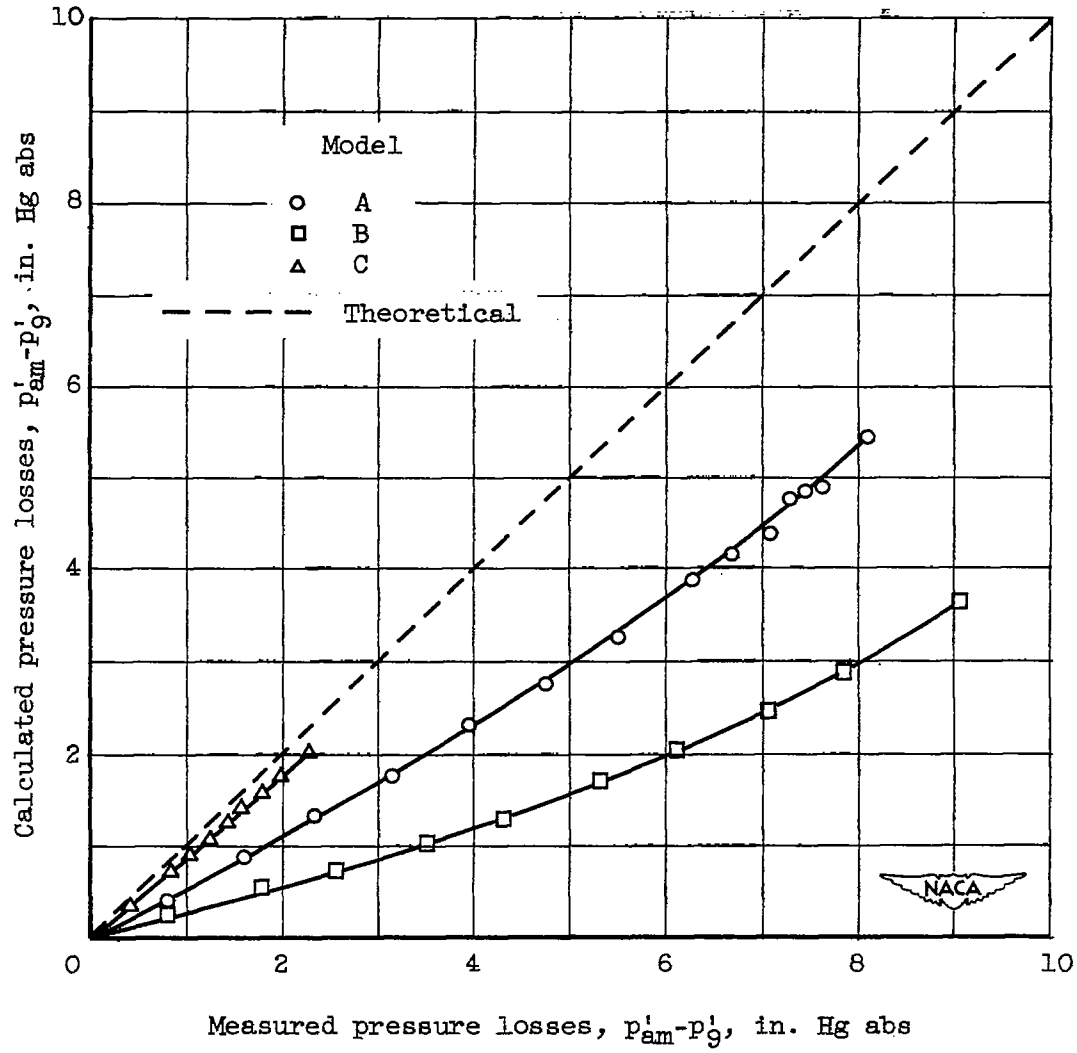


Figure 12. - Comparison of calculated over-all pressure losses with measured over-all pressure losses.



NACA-Langley - 1-12-53 - 400

[redacted]



[redacted]